RUNDC1 Regulates Proinsulin/Insulin Trafficking and TGN Exit

Chau Vuong

A dissertation
submitted in partial fulfillment of the
requirements for the degree of

Doctor of Philosophy

University of Washington
2026

Reading Committee: Michael Ailion, Chair
Alex Merz
Jihong Bai

Program Authorized to Offer Degree:
Biochemistry

University of Washington

Abstract

RUNDC1 Regulates Proinsulin/Insulin Trafficking and TGN Exit

Chau Vuong

Chair of the Supervisory Committee:

Michael Ailion
Department of Biochemistry

Part 1:

The regulated secretion of insulin from pancreatic β-cells is essential for maintaining systemic glucose homeostasis, relying on the highly coordinated sorting and maturation of insulin-containing secretory granules (SGs) at the trans-Golgi network (TGN). However, little information has been obtained about the cytoplasmic regulatory mechanisms controlling the kinetic efficacy of proinsulin export at the TGN. Herein, we have identified RUNDC1, a highly conserved member of the RUN domain family of proteins, as a major factor in regulating proinsulin trafficking in pancreatic β cells. Through RNA interference-mediated knockdown of RUNDC1 in INS-1 derived insulinoma lines, we demonstrate that loss of RUNDC1 significantly impairs glucose-stimulated insulin secretion and reduces fractional insulin release while having no effect on either overall intracellular insulin synthesis or steady-state levels of stored hormone. The secretory defect seen with loss of RUNDC1 is not due to alterations in cargo processing since the expression, localization, and maturation of processing enzymes such as carboxypeptidase E (CPE) and proprotein convertases PC1/3 (PC1/3) are

normal. Immunofluorescence studies show that depletion of RUNDC1 results in an accumulation of newly synthesized proinsulin at the TGN. Using a SNAP-tag-based pulse-chase imaging technique to monitor in real time the kinetic trafficking patterns of newly synthesized cargo, we found that depletion of RUNDC1 delays the kinetic exit of newly formed proinsulin from the TGN. Our collective data indicate that RUNDC1 functions as a critical molecular traffic controller at the TGN and demonstrates that kinetic efficacy of nascent granule formation is required to support the sustained exocytic response to glucose stimulation.

Part 2:

The Rab GTPase RAB-2 is a master regulator of secretory cargo sorting and maturation, yet the precise biochemical mechanisms controlling its molecular switch remain poorly defined. In *C. elegans*, RAB-2 must actively cycle between GTP- and GDP-bound states to facilitate secretory granule (SG) maturation, as both hyperactive and inactive variants phenocopy null mutations. Here, we characterize the biochemical regulation of this cycle by the putative GTPase-activating protein (GAP) TBC-8 and the RAB-2-specific interactor RUND-1. Using in vitro malachite green assays, we provide the first direct biochemical evidence that TBC-8 functions as a potent GAP for RAB-2. We further demonstrate that the TBC-8 TBC domain is structurally sufficient for this activity, forming a stable 1:1 heterodimer with RAB-2 at nanomolar concentrations. We find that RUND-1 serves as a potent inhibitor of TBC-8 GAP activity. Mass photometry confirms that RUND-1 and RAB-2 assemble into complexes, providing a biophysical basis for a model where RUND-1 modulates the accessibility of the GAP to the

GTPase. Our results suggest a role for RUND-1 in fine-tuning RAB-2 signaling longevity by shielding it from TBC-8-mediated hydrolysis.

TABLE OF CONTENTS

ACKNOWLEDGEMENT

I am grateful to my advisor, Michael Ailion, for his mentorship, and sustained support throughout my graduate studies. I also want to thank Amy Clippinger, whose encouragement and mentorship provided vital direction and strength along the way. My sincere thanks go to the members of my thesis committee: Suzanne Hoppins, Alex Merz, Jihong Bai, and Sandra Bajjalieh. Their critical insights and expertise significantly elevated the quality of this research. I also acknowledge the contributions of past Ailion Lab members, Jérôme Cattin-Ortolá, Irini Topalidou and Michael Crawford, whose previous efforts paved the way for these projects. On a personal note, I want to thank Lewis Caro for his exceptional friendship and unwavering support during my time in graduate school. Additionally, I want to recognize Daniel Park, whose persistence in science and shared dedication have been a true inspiration.

CHAPTER 1. GENERAL INTRODUCTION

1.1 FUNDAMENTALS OF THE SECRETORY PATHWAY

The eukaryotic cell is a highly compartmentalized environment separated into distinct, membrane-bound organelles. While this spatial segregation allows for specialized biochemical reactions to occur in isolation, it presents a complex logistical challenge: newly synthesized proteins, lipids, and complex carbohydrates must be accurately routed from their site of origin to their precise functional destinations.

Secretory proteins are first translated by ribosomes at the endoplasmic reticulum (ER). Once translation is complete, secretory protein will move out of the ER and continue its journey through the Golgi stack. Traditional textbook models long depicted this process as a passive transit through static cisternal compartments via forward-moving transport vesicles. However, the emerging consensus in the field favors the cisternal maturation model, which proposes that the cisternae are dynamic structures that progressively mature to carry cargo forward (Losev et al, 2006).

Upon reaching the *trans*-Golgi network (TGN), cargo molecules diverge into two fundamentally distinct transport pathways: the constitutive secretory pathway or the regulated secretory pathway (Caro and Palade, 1964; Jamieson and Palade, 1967).

1.1.1 Constitutive Pathway

The constitutive secretory pathway is an absolute requirement of all eukaryotic cells. It operates continuously and automatically, completely independent of extracellular stimuli (Moore and Kelly, 1985). Vesicles in this pathway load cargo directly from the TGN and move along the cytoskeleton to fuse with the plasma membrane. This default flux serves two primary homeostatic functions: the continuous delivery of newly synthesized lipids and transmembrane proteins required to maintain plasma membrane integrity, and the sustained secretion of extracellular matrix components, soluble signaling factors, and housekeeping proteins. Because transport is continuous, cargo is not stored intracellularly (Moore and Kelly, 1985; Kelly, 1985; Wieland et al, 1987).

1.1.2 The Regulated Pathway

In contrast, the regulated secretory pathway is a highly specialized adaptation restricted to professional secretory cells, such as neurons, exocrine cells, and endocrine tissues. In this pathway, specialized cargo - including neurotransmitters, neuropeptides, peptide hormones, and digestive enzymes - is actively concentrated and packaged into unique, high-capacity storage carriers known as secretory granules or dense-core vesicles (Tooze and Huttner, 1990). Unlike constitutive carriers, these mature granules do not automatically fuse with the plasma membrane upon formation. Instead, they are stably

stored within the cytoplasm, forming an intracellular pool that can be released upon stimulation (Voets et al, 1999).

Exocytosis is strictly gated and occurs only in response to a specific environmental trigger. Typically, an extracellular stimulus (such as a nutrient shift or an incoming action potential) binds to surface receptors, initiating a signaling cascade that triggers a transient influx of intracellular calcium (Bokvist et al, 1995; Ammälä et al, 1995). This local surge in calcium acts on specialized calcium-sensing machinery on the vesicle surface, accelerating the final priming and fusion steps required for rapid, bulk hormone or transmitter release.

Interestingly, while secretory cells make a lot of secretory granules, only a small fraction (1-5%) is released upon physiological stimulation. The popular explanation is that vesicles are segregated into distinct pools based on their physical proximity to the plasma membrane. The readily releasable pool (RRP) consists of granules already docked and primed at the cell surface for immediate exocytosis upon stimulation while the reserve pool resides deeper within the cytoplasm and requires active mobilization along microtubule networks to reach the release sites (Straub et al, 2004). However, the evidence of distinct granule subpopulations and granule age-dependent secretion suggests that granule selection for exocytosis is governed by more complex mechanisms than just proximity to the cell periphery (Rhodes et al, 1987; Duncan et al, 2003; Tsuboi et al, 2010; Kreutzberger et al, 2017).

1.2 THE LIFECYCLE OF A SECRETORY GRANULE: FROM BUDDING TO EXOCYTOSIS

Once a cargo protein is designated for the regulated secretory pathway at the TGN, it enters a highly coordinated, sequential lifecycle. This process transforms a pool of luminal proteins into a densely packed, physically distinct, and highly mobile organelle capable of rapid, stimulus-dependent exocytosis (Farquhar et al, 1978; Verhage et al, 1991; Burgoyne and Morgan, 2003). This structural and functional evolution progresses through three major operational phases: biogenesis at the TGN, post-TGN maturation, and the terminal steps of exocytotic secretion (Castle, 2022).

1.2.1 Granule Formation: Biogenesis at the TGN

The TGN stands as the primary sorting station of the secretory pathway, positioned at the exit face of the Golgi stack to segregate lipid and protein cargo into distinct vesicular carriers (Caro and Palade, 1964; Jamieson and Palade, 1967). In classical cell biology paradigms, the TGN is frequently depicted as a rigid, digital logistics hub - an abrupt intersection where proteins are perfectly partitioned into separate, dedicated transport vesicles destined for the plasma membrane, lysosomes, or secretory granules (SGs).

However, the biogenesis of SGs is a highly dynamic, progressive process. The nascent carriers emanating from the TGN are compositional hybrids. Rather than emerging completely purified, these membranes exit the TGN carrying a heterogeneous mixture of regulated secretory proteins, constitutive trafficking machinery, and lysosomal hydrolases. Consequently, biogenesis at the TGN represents only the hierarchical initiation of a sorting cascade that continues to unfold far into distal post-Golgi compartments (Arvan and Castle, 1998; Castle, 2022).

The foundational framework for soluble protein sorting at the TGN was established in the late 1980s through the discovery of mannose-6-phosphate receptor (M6P-R). M6P-R selectively segregates lysosomal enzymes from other proteins trafficking through the TGN by recognizing and binding to phosphate groups on the terminal mannose residues of N-linked glycans. Through this interaction, the M6P-R physically anchors the hydrolase to the TGN membrane, facilitating its packaging into clathrin-coated vesicles destined for the lysosome (Gabel and Foster, 1986). This model of receptor-mediated sorting sparked a long-standing hypothesis that analogous receptors must exist to direct proteins into the constitutive and regulated secretory pathways. However, there has not been discovery of either conserved sorting motifs on secretory cargo or specific receptors to recognize them. Hence, to understand how cargo is committed to the regulated secretory lineage at the TGN, two competing yet potentially cooperative models were proposed:

- **Active Sorting Model:** This model posits that high-fidelity cargo selection occurs strictly at the physical boundary of the TGN during the fission of the nascent vesicle. According to this framework, specific molecular sorting receptors or gated physical barriers actively exclude constitutive secretory proteins and lysosomal enzymes from entering the budding SG from the outset. For example, phogrin is a major transmembrane component crucial to the identity of pancreatic beta-cell and pituitary granules. To ensure it is gathered into the regulated pathway as the vesicle buds, phogrin relies on a cytosolic, leucine-based sorting signal. This specific motif interacts directly with the clathrin adaptor protein AP-1 *in vitro*. This demonstrates that clathrin-coated machinery at the TGN face acts as an active gatekeeper, physically capturing and concentrating phogrin into the budding vesicle (Torii et al, 2005).
- **Passive Sorting Model:** This model argues that individual receptor binding is unnecessary for bulk cargo. Instead, sorting is driven by the intrinsic biophysical properties of the cargo itself - namely, its ability to undergo condensation or liquid-liquid phase separation (LLPS) in the acidic, high-calcium environment of the TGN/immature granule. For example, chromogranin B utilizes its intrinsically disordered N-terminal domain to drive formation of fluid condensates which con

recruit soluble clients like proinsulin. Consequently, proteins capable of participating in these interactions are consolidated within the maturing granule, while non-aggregating proteins remain soluble at the periphery, left exposed to downstream vesicular pruning machinery (Bearrows et al, 2019; Parchure et al, 2022).

Accumulating evidence indicates that TGN biogenesis relies on a hybrid mechanism where elements of both models cooperate. The initial segregation of bulk luminal cargo is balanced by highly specific, motif-directed entry of critical membrane-associated components.

1.2.2 Granule Maturation: Post-TGN Processing and Refinement

Once immature secretory granules (ISGs) undergo fission from the TGN, they enter a maturation phase. This post-TGN stage transforms a non-selective, compositional hybrid carrier into a highly condensed, stimulus-responsive, and functionally competent mature SGs. The maturation process relies on a tightly coordinated network of physical structural remodeling, proteolytic processing, and selective vesicular recycling.

Homotypic ISG Fusion

Early morphological studies demonstrate that newly generated ISGs are relatively small as they emerge from the TGN. Classic morphological and real-time imaging studies demonstrate that early post-TGN compartments often appear as irregularly shaped granules, featuring several distinct foci of condensed secretory content. As maturation progresses, these evolve into larger, uniformly spherical profiles surrounding a single, consolidated core mass (Farquhar et al, 1978; Salpeter et al, 1981; Tooze et al, 1991).

Ex vivo reconstitution and in vivo models have confirmed that this volume increase can be driven by homotypic IG-IG fusion, a process mediated by specific proteins including HID-1 and syntaxin6 (Wendler et al, 2001; Du et al, 2016). However, whether homotypic fusion is an absolute, universal requirement for granule maturation requires further testing. Deciphering the strict necessity of homotypic fusion in situ is further complicated by concurrent membrane events as IGs simultaneously undergo heterotypic fusion with incoming transport vesicles arriving from the Golgi or endosomal networks to deliver late-stage maturation factors (Topalidou et al, 2016).

Proteolytic Cargo Processing

Many secretory cargo molecules are synthesized as inactive precursors. Within the acidic interior of the IG, co-packaged proenzymes (such as proprotein convertases and carboxypeptidases) undergo self-cleavage and activation. Luminal processing enzymes, such as prohormone convertases (PC1/3 and PC2) and Carboxypeptidase E (CPE), are

co-packaged with proinsulin or pro-hormones at the TGN but remain enzymatically dormant at higher pH levels (Furuta et al 1997; Zhu et al, 2002; Meier et al, 2022; Chen, 2023). As the v-ATPase lowers the luminal pH, these proteases undergo auto-activation and systematically cleave the extended precursor molecules into biologically active, shorter peptides (e.g., cleaving proinsulin into mature insulin and C-peptide).

This cleavage alters the physical chemistry of the cargo. For example, insulin typically has a much lower solubility under acidic conditions, allowing it to condense and crystallize into an insoluble, highly concentrated crystalline core in the presence of zinc ions. This matrix condensation relieves osmotic pressure within the granule, allowing clathrin-coated vesicles to bud off excess membrane, resulting in the characteristic compact, electron-dense appearance of the mature SGs (Dunn, 2005; Landreh et al, 2012).

Vesicular Retrieval and Membrane Protein Remodeling

Another requirement for transforming an ISG into a functionally competent, stimulus-responsive organelle is the drastic biochemical refinement of its membrane. While ISGs exit the trans-Golgi Network (TGN) as compositional hybrids, the mature granule membrane must be strictly stripped of transient biogenesis machinery, non-granule trafficking components, and mistargeted proteins.

During this post-TGN maturation phase, the surface of the IG is heavily studded with clathrin-coated vesicular buds that function as a selective exit filtration system (Tooze, J., and S. A. Tooze, 1986). Here, the cytosolic coat adaptor AP-1 actively clusters and evacuates transient proteins - such as mannose-6-phosphate receptors (MPRs), and the processing protease furin (Dittié et al, 1997; Klumperman et al, 1998). Conversely, granule-resident proteins like phogrin and ICA512 maintained a stable concentration either through signal-mediated retention or by simply lacking the motifs required to engage in the AP-1 machinery.

1.2.3 Granule Secretion

Following the post-trans-Golgi network maturation phase, functionally competent secretory granules must navigate the crowded cytoplasmic landscape to reach the cell periphery for regulated exocytosis. This final stage of the secretory pathway involves a highly coordinated transition from long-range intracellular transport to localized cytoskeletal remodeling at the plasma membrane, culminating in a stimulus-dependent fusion event.

Microtubule-Mediated Cytoplasmic Translocation

Because mature granules are synthesized near the perinuclear region of the cell, they require an active transport network to traverse the distance to the plasma membrane.

This long-range translocation through the cytoplasm is mediated by dense tracks of the microtubule cytoskeleton. Experimental evidence in endocrine lineages, such as AtT-20 anterior pituitary cells, confirms that endocrine systems rely on a similar microtubule-dependent transport paradigm for granule delivery (Tooze et al, 1987; Kreis et al, 1989).

Docking and Priming

Upon reaching the cell periphery, granules are systematically organized into distinct functional pools. A small fraction is mobilized to form the Readily Releasable Pool (RRP)—granules that are physically positioned directly adjacent to the plasma membrane (Daniel et al, 1999; Barg et al, 2002).

Once docked, the granule must undergo an ATP-dependent biochemical priming step. During priming, the vesicular SNARE protein (v-SNARE, such as VAMP2) begins to partially interlock with corresponding target SNARE proteins on the plasma membrane (t-SNAREs, such as Syntaxin 1 and SNAP-25) (Knowles et al, 2010; Yin et al, 2018). This partial assembly forms a highly strained, intermediate trans-SNARE complex, effectively positioning the fusion machinery into pre-zippered state.

Exocytotic Fusion

The granule remains stably paused in this primed state until an extracellular stimulus triggers a local influx of intracellular calcium. Upon receiving an extracellular stimulatory signal, a localized influx of calcium rapidly elevates the concentration of divalent cations in the immediate environment. This influx is sensed by specialized vesicle-associated calcium sensors, the most important of which are members of the synaptotagmin family. Upon calcium binding, synaptotagmins undergo a conformational change that drives the fully assembled v-SNARE and t-SNARE proteins to complete their zippering action and may also perturb the membranes to promote the onset of fusion (Tucker et al, 2004; Kreutzberger et al, 2017; Kiessling et al, 2018). This immense physical pulling force overcomes electrostatic repulsion of the hydration shell, and membrane bending energy, forcing the granule membrane and the plasma membrane to fuse.

1.3 THE RAB-2 PATHWAY IN SECRETORY GRANULE BIOGENESIS

The RAB-2 (worm) GTPase has been shown to act as a master regulator of SG biogenesis. While originally characterized for its role in endoplasmic reticulum-to-Golgi transport (Tisdale et al, 1992), elegant forward genetic screens in *Caenorhabditis elegans* neurons - and subsequent validations in mammalian pancreatic β-cells - have revealed that RAB-2 commands a highly specialized, post-Golgi molecular network (Sumakovic et al, 2009; Edwards et al, 2009; Sugawara et al, 2014; Matsunaga et al 2017). Loss of RAB-2 function results in a severe sorting defect: secretory cargoes are missorted into late endosomal-lysosomal markers, leading to a reduction of secretory cargos in secretory granules. Despite this depletion, neither proprotein processing nor

the exocytic machinery is impaired, allowing these content-poor granules to undergo release in *C. elegans* neurons.

The execution of the RAB-2 pathway relies on a highly coordinated multi-protein circuit consisting of specialized effectors, adaptors, and recycling machinery:

The EARP Recycling Complex

The pathway integrates the Endosome-Associated Recycling Protein (EARP) complex, whose membrane interaction is strictly enabled by the partner protein EIPR-1 (Topalidou et al, 2016). In the RAB-2 pathway, the cargo loss caused by *rab-2* mutations can be rescued by expressing a dominant-active form of RAB-5 (Q78L) which blocks endosomal fusion (Sumakovic et al, 2009). This genetic rescue demonstrates that cargo retention during granule formation and maturation relies on a dynamic interaction between endosomes and secretory granules. Structurally, the EARP complex shares a striking resemblance to the Golgi-associated retrograde protein (GARP) complex, which traditionally supports endosome-to-TGN retrograde transport (Conibear et al, 2003). The identification of EARP as a key player in this process enhances our understanding of dense-core vesicle biogenesis: it reveals that generating a mature granule depends not just on the initial packaging of cargo as it buds from the *trans*-Golgi, but also on the active retrieval and recycling of cargo and essential sorting factors from the endosomal compartment.

GTPase Activating Proteins (GAPs)

The temporal regulation and hydrolysis of Rab2 activity are controlled by its putative GAP TBC-8. Genetic analysis in *C. elegans* reveals that *tbc-8* and *rab-2* operate within the same genetic pathway. Furthermore, TBC-8 directly influences RAB-2 membrane recruitment *in vivo:* while active RAB-2 typically localizes to discrete puncta at the Golgi apparatus, overexpressing TBC-8 redistributes RAB-2 into the cytosol, a phenotype characteristic of its inactive, GDP-bound state. However, because obtaining soluble TBC-8 protein for *in vitro* assays has proven difficult, direct biochemical confirmation of its GAP activity toward RAB-2 remains to be definitively demonstrated, leaving open the possibility that TBC-8 may target an alternative Rab GTPases. (Hannemann et al, 2012).

Tethering and Other Effectors

RAB-2 coordinates cargo retention and sorting by organizing a sophisticated network of tethering and scaffolding effectors. One of them is CCCP-1, which interacts exclusively with RAB-2 and likely acts as an independent effector (Ailion et al, 2014). Like classic golgins, CCCP-1 possesses an elongated, oligomeric, and predominantly coiled-coil

architecture, and it utilizes its C-terminal domain to anchor directly to the trans-Golgi membrane (Gillingham and Munro, 2016; Cattin-Ortolá et al, 2017). This structural profile suggests that CCCP-1 may function as a molecular tether, extending its N-terminus into the cytoplasm to capture incoming membrane carriers and facilitate the specialized fusion events required during SG biogenesis. However, the precise identity of the incoming membrane compartments remains to be determined.

Discovered at the same time with CCCP-1 in *C. elegans*, the literature surrounding RUND-1 has not been updated in over a decade (Ailion et al, 2014). Early foundational findings regarding its function relied heavily on assays utilizing exogenous, overexpressed dense-core vesicle cargoes in neuronal models, leaving its role on endogenous secretory cargoes largely uncharacterized.

RUND-1 is highly conserved across species and acts as a central coordinating centerpiece for effector assembly, directly interacting with RAB-2 and other RAB-2 effectors such as RIC-19 and TBC-8 (Sumakovic et al, 2009; Hannemann et al, 2012; Ailion et al, 2014). Structurally, the protein is defined by two coiled-coil domains and a highly conserved C-terminal RUN (RPIP8/UNC-14/NESCA) domain. Functional domain mapping has revealed that the RUN domain of RUND-1 is entirely sufficient to mediate both its localization to the Golgi apparatus and its physical interaction with GTP-bound RAB-2. However, this domain alone is insufficient to sustain SG biogenesis as expressing only the RUN domain fails to rescue the severe secretory cargo missorting defects observed in *rund-1* mutant worms. While the RUN domain serves as the essential membrane targeting and GTPase-binding site, the remaining conserved structural regions of the protein - such as the coiled-coil domains - are required for RUND-1 function. Given that mammalian RUNDC1 shares these highly conserved domain architectures, understanding how these distinct structural regions coordinate sorting platforms is a central focus of this thesis, which investigates the role of rat RUNDC1 during regulated insulin secretion in pancreatic β-cell (INS-1 832/13 cell lines) models.

1.4 REFERENCES

Ailion, Michael, et al. "Two Rab2 Interactors Regulate Dense-Core Vesicle Maturation." *Neuron*, vol. 82, no. 1, 2 Apr. 2014, pp. 167-80, https://doi.org/10.1016/j.neuron.2014.02.017.

Ammälä, Carina, et al. "Exocytosis Elicited by Action Potentials and Voltage-Clamp Calcium Currents in Individual Mouse Pancreatic B-Cells." *The Journal of Physiology*, vol. 472, no. 1, 1993, pp. 645-59, https://doi.org/10.1113/jphysiol.1993.sp019966.

Arvan, Peter, and J. David Castle. "Sorting and Storage During Secretory Granule Biogenesis: Looking Backward and Looking Forward." *Biochemical Journal*, vol. 332, no. 3, 15 June 1998, pp. 593-610, https://doi.org/10.1042/bj3320593.

Barg, Sebastian, et al. "A Subset of 50 Secretory Granules in Close Contact with L-Type Ca2+ Channels Accounts for First-Phase Insulin Secretion in Mouse Beta-Cells." *Diabetes*, vol. 51, no. suppl 1, Feb. 2002, pp. S74-S82, https://doi.org/10.2337/diabetes.51.2007.s74.

Bearrows, Steven C., et al. "Chromogranin B Regulates Early-Stage Insulin Granule Trafficking from the Golgi in Pancreatic Islet β-Cells." *Journal of Cell Science*, vol. 132, no. 13, 1 July 2019, https://doi.org/10.1242/jcs.231373.

Bokvist, Krister, et al. "Co-Localization of L-Type Ca2+ Channels and Insulin-Containing Secretory Granules and Its Significance for the Initiation of Exocytosis in Mouse Pancreatic B-Cells." *The EMBO Journal*, vol. 14, no. 1, 1995, pp. 50-57, https://doi.org/10.1002/j.1460-2075.1995.tb06974.x.

Burgoyne, Robert D., and Alan Morgan. "Secretory Granule Exocytosis." *Physiological Reviews*, vol. 83, no. 2, 1 Apr. 2003, pp. 581-632, https://doi.org/10.1152/physrev.00031.2002.

Caro, Lucien G., and George E. Palade. "Protein Synthesis, Storage, and Discharge in the Pancreatic Exocrine Cell: An Autoradiographic Study." *Journal of Cell Biology*, vol. 20, no. 3, Mar. 1964, pp. 473-95, https://doi.org/10.1083/jcb.20.3.473.

Castle, J. David. "Biogenesis of Secretory Granules." *Exocytosis: From Molecules to Cells*, IOP Publishing, 2022, pp. 2-1-2-51.

Cattin-Ortolá, Jérôme, et al. "CCDC186 Controls Dense-Core Vesicle Cargo Sorting by Exit." *bioRxiv*, 2019, https://doi.org/10.1101/616458.

Cattin-Ortolá, Jérôme, et al. "The Dense-Core Vesicle Maturation Protein CCCP-1 Binds RAB-2 and Membranes Through Its C-Terminal Domain." *Traffic*, vol. 18, no. 11, Nov. 2017, pp. 720-32, https://doi.org/10.1111/tra.12507.

Chen, Yan Chen, et al. "Deletion of Carboxypeptidase E in β-Cells Disrupts Proinsulin Processing but Does Not Lead to Spontaneous Development of Diabetes in Mice." *Diabetes*, vol. 72, no. 9, 1 Sept. 2023, pp. 1277-88, https://doi.org/10.2337/db22-0945.

Conibear, Elizabeth, et al. "Vps51p Mediates the Association of the GARP (Vps52/53/54) Complex with the Late Golgi t-SNARE Tlg1p." *Molecular Biology of the Cell*, vol. 14, no. 4, Apr. 2003, pp. 1610-23, https://doi.org/10.1091/mbc.e02-10-0654.

Daniel, S., et al. "Identification of the Docked Granule Pool Responsible for the First Phase of Glucose-Stimulated Insulin Secretion." *Diabetes*, vol. 48, no. 9, 1 Sept. 1999, pp. 1686-90, https://doi.org/10.2337/diabetes.48.9.1686.

Dean, P. M. "Ultrastructural Morphometry of the Pancreatic β-Cell." *Diabetologia*, vol. 9, no. 2, 1973, pp. 115-19, https://doi.org/10.1007/BF01230690.

Dittié, Amely S., et al. "Interaction of Furin in Immature Secretory Granules from Neuroendocrine Cells with the AP-1 Adaptor Complex Is Modulated by Casein Kinase II Phosphorylation." *The EMBO Journal*, vol. 16, no. 16, 15 Aug. 1997, pp. 4859-70, https://doi.org/10.1093/emboj/16.16.4859.

Du, W., et al. "HID-1 Is Required for Homotypic Fusion of Immature Secretory Granules During Maturation." *eLife*, vol. 5, 18 Oct. 2016, p. e18134, https://doi.org/10.7554/eLife.18134.

Duncan, Rory, et al. "Functional and Spatial Segregation of Secretory Vesicle Pools According to Vesicle Age." *Nature*, vol. 422, no. 6928, 2003, pp. 176–180, https://doi.org/10.1038/nature01389.

Dunn, Michael F. "Zinc-Ligand Interactions Modulate Assembly and Stability of the Insulin Hexamer -- A Review." *Biometals*, vol. 18, no. 4, Aug. 2005, pp. 295-303, https://doi.org/10.1007/s10534-005-3685-y.

Edwards, Stacey L., et al. "Impaired Dense Core Vesicle Maturation in Caenorhabditis Elegans Mutants Lacking Rab2." *Journal of Cell Biology*, vol. 186, no. 6, 21 Sept. 2009, pp. 881-95, https://doi.org/10.1083/jcb.200902095.

Farquhar, Marilyn G., et al. "Intracellular Transport and Packaging of Prolactin: A Quantitative Electron Microscope Autoradiographic Study of Mammotrophs Dissociated

from Rat Pituitaries." *Endocrinology*, vol. 102, no. 1, 1 Jan. 1978, pp. 296-311, https://doi.org/10.1210/endo-102-1-296.

Furuta, M., et al. "Defective Prohormone Processing and Altered Pancreatic Islet Morphology in Mice Lacking Active SPC2." *Proceedings of the National Academy of Sciences*, vol. 94, no. 13, 24 June 1997, pp. 6646-51, https://doi.org/10.1073/pnas.94.13.6646.

Gabel, Christopher A., and Foster S. A. "Lysosomal Enzyme Trafficking in Mannose 6-Phosphate Receptor-Positive Mouse L-Cells: Demonstration of a Steady State Accumulation of Phosphorlyated Acid Hydrolases." *The Journal of Cell Biology*, vol. 102, no. 3, 1 Mar. 1986, pp. 943-50, https://doi.org/10.1083/jcb.102.3.943.

Gillingham, Alison K., and Sean Munro. "Finding the Golgi: Golgin Coiled-Coil Proteins Show the Way." *Trends in Cell Biology*, vol. 26, no. 6, June 2016, pp. 399-408, https://doi.org/10.1016/j.tcb.2016.02.005.

Hannemann, Maike, et al. "TBC-8, a Putative RAB-2 GAP, Regulates Dense Core Vesicle Maturation in Caenorhabditis Elegans." *PLoS Genetics*, vol. 8, no. 5, 24 May 2012, p. e1002722, https://doi.org/10.1371/journal.pgen.1002722.

Jamieson, James D., and George E. Palade. "Intracellular Transport of Secretory Proteins in the Pancreatic Exocrine Cell: I. Role of the Peripheral Elements of the Golgi Complex." *Journal of Cell Biology*, vol. 34, no. 2, 1 Aug. 1967, pp. 577-96, https://doi.org/10.1083/jcb.34.2.577.

Kelly, Regis B. "Pathways of Protein Secretion in Eukaryotes." *Science*, vol. 230, no. 4721, 1985, pp. 25-32, https://doi.org/10.1126/science.2994224.

Kiessling, V., et al. "A Molecular Mechanism for Calcium-Mediated Synaptotagmin-Triggered Exocytosis." *Nature Structural & Molecular Biology*, vol. 25, no. 10, Oct. 2018, pp. 911–17, https://doi.org/10.1038/s41594-018-0130-9.

Klumperman, Judith, et al. "Mannose 6-Phosphate Receptors Are Sorted from Immature Secretory Granules via Adaptor Protein AP-1, Clathrin, and Syntaxin 6-Positive Vesicles." *Journal of Cell Biology*, vol. 141, no. 2, 20 Apr. 1998, pp. 359-71, https://doi.org/10.1083/jcb.141.2.359.

Knowles, Michelle K., et al. "Single Secretory Granules of Live Cells Recruit Syntaxin-1 and Synaptosomal Associated Protein 25 (SNAP-25) in Large Copy Numbers." *Proceedings of the National Academy of Sciences*, vol. 107, no. 48, 30 Nov. 2010, pp. 20810-15, https://doi.org/10.1073/pnas.1014840107.

Kreis, Thomas E., et al. "Secretory Granules and Endosomes Show Saltatory Movement Biased to the Anterograde and Retrograde Directions, Respectively, Along Microtubules in AtT20 Cells." *European Journal of Cell Biology*, vol. 49, no. 1, June 1989, pp. 128-39.

Kreutzberger, Alex J B et al. “Distinct insulin granule subpopulations implicated in the secretory pathology of diabetes types 1 and 2.” eLife vol. 9 e62506. 9 Nov. 2020, doi:10.7554/eLife.62506.

Kreutzberger, Alex J. B., et al. "Reconstitution of Calcium-Mediated Exocytosis of Dense-Core Vesicles." *Science Advances*, vol. 3, no. 7, Jul. 2017, p. e1603208, https://doi.org/10.1126/sciadv.1603208.

Landreh, Michael, et al. "Insulin Solubility Transitions by pH-Dependent Interactions with Proinsulin C-Peptide." *FEBS Journal*, vol. 279, no. 24, 2012, pp. 4589-97, https://doi.org/10.1111/febs.12045.

Losev, Elena, et al. "Golgi Maturation Visualized in Living Yeast." *Nature*, vol. 441, no. 7096, 22 June 2006, pp. 1002-06, https://doi.org/10.1038/nature04717.

Matsunaga, Kyoko, et al. "Rab2a and Rab27a Cooperatively Regulate the Transition from Granule Maturation to Exocytosis Through the Dual Effector Noc2." *Journal of Cell Science*, vol. 130, no. 3, 1 Feb. 2017, pp. 541-50, https://doi.org/10.1242/jcs.195479.

Meier, Danielle T., et al. "Prohormone Convertase 1/3 Deficiency Causes Obesity Due to Impaired Proinsulin Processing." *Nature Communications*, vol. 13, no. 1, 13 Aug. 2022, p. 4761, https://doi.org/10.1038/s41467-022-32509-4.

Moore, Hsiao-Ping, and Regis B. Kelly. "Secretory Protein Targeting in a Pituitary Cell Line: Differential Transport of Foreign Secretory Proteins to Distinct Secretory Pathways." *Journal of Cell Biology*, vol. 101, no. 5 Pt 1, Nov. 1985, pp. 1773-81, https://doi.org/10.1083/jcb.101.5.1773.

Muller, Lloyd, and Iris Lindberg. "The Cell Biology of the Prohormone Convertases PC1 and PC2." *Progress in Nucleic Acid Research and Molecular Biology*, vol. 63, 1999, pp. 69-108, https://doi.org/10.1016/s0079-6603(08)60720-5.

Orci, Lelio, et al. "Conversion of Proinsulin to Insulin Occurs Coordinately with Acidification of Maturing Secretory Vesicles." *Journal of Cell Biology*, vol. 103, no. 6 Pt 1, Dec. 1986, pp. 2273-81, https://doi.org/10.1083/jcb.103.6.2273.

Parchure, Aniruddha, et al. "Liquid-Liquid Phase Separation Facilitates the Biogenesis of Secretory Storage Granules." *Journal of Cell Biology*, vol. 221, no. 12, 5 Dec. 2022, p. e202206132, https://doi.org/10.1083/jcb.202206132.

Rhodes, Christopher J., and Pierre A. Halban. "Newly Synthesized Proinsulin/Insulin and Stored Insulin Are Released from Pancreatic B Cells Predominantly via a Regulated, Rather than a Constitutive, Pathway." *The Journal of Cell Biology*, vol. 105, no. 1, 1987, pp. 145-53, https://doi.org/10.1083/jcb.105.1.145.

Salpeter, M. M., and Marilyn G. Farquhar. "High Resolution Analysis of the Secretory Pathway in Mammotrophs of the Rat Anterior Pituitary." *Journal of Cell Biology*, vol. 91, no. 1, Oct. 1981, pp. 240-46, https://doi.org/10.1083/jcb.91.1.240.

Straub, Susanne G., et al. "Stimulation of Insulin Release by Glucose Is Associated with an Increase in the Number of Docked Granules in the Beta-Cells of Rat Pancreatic Islets." *Diabetes*, vol. 53, no. 12, 2004, pp. 3179-83, https://doi.org/10.2337/diabetes.53.12.3179.

Sugawara, T., et al. "Rab2A Is a Pivotal Switch Protein That Promotes Either Secretion or ER-Associated Degradation of (Pro)insulin in Insulin-Secreting Cells." *Scientific Reports*, vol. 4, 2014, p. 6952, https://doi.org/10.1038/srep06952.

Sumakovic, Marija, et al. "UNC-108/RAB-2 and Its Effector RIC-19 Are Involved in Dense Core Vesicle Maturation in Caenorhabditis Elegans." *Journal of Cell Biology*, vol. 186, no. 6, 21 Sept. 2009, pp. 897-914, https://doi.org/10.1083/jcb.200902096.

Tisdale, E. J., et al. "GTP-Binding Mutants of Rab1 and Rab2 Are Potent Inhibitors of Vesicular Transport from the Endoplasmic Reticulum to the Golgi Complex." *The Journal of Cell Biology*, vol. 119, no. 4, Nov. 1992, pp. 749-61, https://doi.org/10.1083/jcb.119.4.749.

Tooze, John, and Brian Burke. "Accumulation of Adrenocorticotropin Secretory Granules in the Midbody of Telophase AtT20 Cells: Evidence that Secretory Granules Move Anterogradely Along Microtubules." *Journal of Cell Biology*, vol. 104, no. 4, Apr. 1987, pp. 1047-57, https://doi.org/10.1083/jcb.104.4.1047.

Tooze, J., and S. A. Tooze. "Clathrin-Coated Vesicular Transport of Secretory Proteins During the Formation of ACTH-Containing Secretory Granules in AtT20 Cells." *The Journal of Cell Biology*, vol. 103, no. 3, Sept. 1986, pp. 839-50, https://doi.org/10.1083/jcb.103.3.839.

Tooze, Sharon A., and Wieland B. Huttner. "Cell-Free Protein Sorting to the Regulated and Constitutive Secretory Pathways." *Cell*, vol. 60, no. 5, 1990, pp. 837-47, https://doi.org/10.1016/0092-8674(90)90098-W.

Tooze, Sharon A., et al. "Characterization of the Immature Secretory Granule, an Intermediate in Granule Biogenesis." *Journal of Cell Biology*, vol. 115, no. 6, Dec. 1991, pp. 1491-503, https://doi.org/10.1083/jcb.115.6.1491.

Topalidou, Irini, et al. "The EARP Complex and Its Interactor EIPR-1 Are Required for Cargo Sorting to Dense-Core Vesicles." *PLoS Genetics*, vol. 12, no. 5, 18 May 2016, p. e1006074, https://doi.org/10.1371/journal.pgen.1006074.

Torii, Seiji, et al. "Cytoplasmic Transport Signal Is Involved in Phogrin Targeting and Localization to Secretory Granules." *Traffic*, vol. 6, no. 12, Dec. 2005, pp. 1213-24, https://doi.org/10.1111/j.1600-0854.2005.00353.x.

Tsuboi, Takashi, et al. "Age-Dependent Preferential Dense-Core Vesille Exocytosis in Neuroendocrine Cells Revealed by Newly Developed Monomeric Fluorescent Timer Protein." *Molecular Biology of the Cell*, vol. 21, no. 1, 2010, pp. 87-94, https://doi.org/10.1091/mbc.e09-08-0722.

Tucker, Ward C., et al. "Reconstitution of Ca2+-Regulated Membrane Fusion by Synaptotagmin and SNAREs." *Science*, vol. 304, no. 5669, Apr. 2004, pp. 435-38, https://doi.org/10.1126/science.1097196.

Verhage, Matthijs, et al. "Differential Release of Amino Acids, Neuropeptides, and Catecholamines from Isolated Nerve Terminals." *Neuron*, vol. 6, no. 4, Apr. 1991, pp. 517-24, https://doi.org/10.1016/0896-6273(91)90054-4.

Voets, Thomas, et al. "Mechanisms Underlying Phasic and Sustained Secretion in Chromaffin Cells from Mouse Adrenal Slices." *Neuron*, vol. 23, no. 3, July 1999, pp. 607-15, https://doi.org/10.1016/s0896-6273(00)80812-0.

Wendler, Franz, et al. "Homotypic Fusion of Immature Secretory Granules During Maturation Requires Syntaxin 6." *Molecular Biology of the Cell*, vol. 12, no. 6, June 2001, pp. 1699-709, https://doi.org/10.1091/mbc.12.6.1699.

Wieland, Felix T., et al. "The Rate of Bulk Flow from the Endoplasmic Reticulum to the Cell Surface." *Cell*, vol. 50, no. 2, 17 July 1987, pp. 289-300, https://doi.org/10.1016/0092-8674(87)90224-8.

Yin, Phing-Chieh, et al. "Syntaxin Clusters at Secretory Granules in a Munc18-Bound Conformation." *Molecular Biology of the Cell*, vol. 29, no. 22, 1 Nov. 2018, pp. 2700-08, https://doi.org/10.1091/mbc.E17-09-0541.

Zhu, Xiaorong, et al. "Severe Block in Processing of Proinsulin to Insulin Accompanied by Elevation of Des-64,65 Proinsulin Intermediates in Islets of Mice Lacking Prohormone Convertase 1/3." *Proceedings of the National Academy of Sciences*, vol. 99, no. 16, 2002, pp. 10299-304, https://doi.org/10.1073/pnas.162352799.

CHAPTER 2. RUNDC1 REGULATES PROINSULIN/INSULIN TRAFFICKING AND TGN EXIT

2.1 Introduction

Regulation of insulin secretion from pancreatic β-cells is a tightly controlled process that ensures the body maintains blood sugar homeostasis. Insulin is produced in the β-cell's endoplasmic reticulum and then traffics to the trans-Golgi network (TGN) before it can be sorted into immature secretory granules (Orci, 1982; Orci, Ravazzola, and Perrelet, 1984; Arvan and Halban, 2004). Subsequently, proinsulin is cleaved by enzymes including prohormone convertases 1/3 (PC1/3) and carboxypeptidase E (CPE) into the mature forms of insulin and C-peptide (Jackson, Creemers, Ohagi et al., 1997; Naggert, Fricker, Varlamov et al., 1995; Chen et al., 2023). Mature insulin and C-peptide are released via the regulated secretory pathway in response to elevated glucose.

A distinguishing feature of how β-cells function is that they selectively use newly synthesized "young" insulin granules near the plasma membrane, rather than using older granules that have been stored for longer periods of time (Gold G et al., 1982; Ivanova et al., 2013). These young granules are rapidly transported to a Readily Releasable Pool (RRP) at the plasma membrane so that they can support the initial phase response to increased glucose concentrations (Olofsson, Göpel, Barg et al., 2002). Disruptions in either the sorting or exporting mechanisms at the TGN will prevent newly synthesized proinsulin from entering the regulated pathway. Hence, the dynamic kinetics of cargo exit from the TGN, rather than just the total steady-state storage of insulin, dictates the β-cell's capacity to respond to acute glycemic challenges.

Disruptions in this highly coordinated sorting and maturation pathway are central to the pathogenesis of type 2 diabetes (T2D) (Halban et al., 2014). β-cell dysfunction in T2D involves a loss of the first phase of glucose stimulated insulin secretion, along with elevated basal secretion (Ward et al., 1984). While several key components involved in the secretion of SGs include SNARE proteins and accessory tethers (Qin et al, 2017; Zhu et al, 2012; Zhu et al, 2015), little is currently known about the molecular machinery responsible for facilitating early cargo sorting at the TGN. Specifically, the identity of molecular machinery that facilitates the rapid transit of newly synthesized cargo into the regulated pathway is a major outstanding question in endocrine cell biology.

Evolutionary precursors to the insulin sorting machinery have been partially illuminated in simpler model organisms. In *Caenorhabditis elegans*, RUN-domain containing protein RUND-1 (orthologue of mammalian RUNDC1) was shown to be a critical RAB-2 effector acting at the TGN to regulate normal dense core vesicle (DCV) cargo sorting (Ailion et al., 2014). While *rund-1* worm mutants produce morphologically normal DCVs, these

vesicles lack both luminal and transmembrane cargoes, indicating a conserved role for RUNDC1/RUND-1 in early cargo packaging.

Herein, we show that RUNDC1 functions as a rate limiting factor in proinsulin trafficking in pancreatic β-cells. siRNA-mediated reduction of RUNDC1 expression in INS-1 derived 832/13 insulinoma cells and demonstrated that this resulted in significantly reduced glucose-stimulated insulin secretion (GSIS) and decreased fractional insulin release. Importantly, this impairment did not arise from impaired insulin production nor from loss of processing machinery such as CPE or PC1/3. Rather, immunofluorescence analysis revealed a blockade in the TGN where proinsulin accumulated resulting in an overflow of precursor cargo into the constitutive secretory pathway. Consequently, the basal leakage of proinsulin was significantly elevated. Finally, SNAP-tagged pulse chase microscopy provided direct kinetic evidence demonstrating that RUNDC1 is required for timely export of proinsulin from the TGN. In the absence of RUNDC1, newly synthesized proinsulin was retained at the TGN, thereby providing a mechanistic explanation for why GSIS fails. Our data collectively define RUNDC1 as a traffic controller at the TGN that regulates delivery of newly synthesized cargo to the regulated secretory pathway to ensure proper maintenance of systemic glucose balance.

2.2 Result

1. RUNDC1 is required for glucose-stimulated insulin secretion in beta-cells

To study the role of RUNDC1 in pancreatic beta cell activity, we treated the rat insulinoma 832/13 cells with two different siRNAs (siRUNDC1_1 and siRUNDC1_2) to knockdown RUNDC1. Control groups are WT cells and cells treated with non-targeting siRNA (Figure S1). Quantitative PCR confirmed a reduction in RUNDC1 mRNA levels of approximately 70 - 80% compared to control groups (Figure 1A).

Prior work in *C. elegans* showed that *rund-1* mutants exhibit reduced levels of secretory cargo within mature SGs (Ailion et al, 2014). We reasoned that knocking down RUNDC1 in INS-1 cells would similarly affect insulin granule abundance or distribution. Hence, we examined the subcellular localization of insulin using immunofluorescence microscopy. In control cells, insulin primarily localizes to the perinuclear area - representing newly budded granules - as well as distinct puncta distributed throughout the cytosol, characteristic of mature secretory granules. This distribution was preserved in RUNDC1 knockdown cells (Figure 1B), initially suggesting that RUNDC1 knockdown does not cause defects in insulin trafficking. However, because insulin granules have a long half-life of 3 - 5 days, the pre-existing pool of older granules present before the 3-day siRNA knockdown could mask potential biogenesis or trafficking defects in the static immunofluorescence assay. Because beta cells preferentially mobilize and

secrete a younger population of insulin granules upon stimulation, evaluating glucose-stimulated insulin secretion provides a more sensitive readout to test whether RUNDC1 regulates insulin granules.

In WT and non-targeting siRNA controls, increasing glucose concentration from 2.8 mM to 20 mM significantly increased insulin secretion as expected (Figure 1C). However, knockdown of RUNDC1 blunted the secretory response, with insulin release levels remaining significantly lower than controls during glucose stimulation (Figure 1C). We observed no change in basal insulin secretion (Figure 1C). Total intracellular insulin as measured by ELISA showed no significant variation between the groups (Figure 1C), suggesting that the decrease in insulin secretion did not stem from reduced synthesis. When normalized as a percentage of total insulin content, *Rundc1*KD cells exhibited a sharp decrease in fractional secretion, with values dropping from approximately 0.8 - 0.9% in controls to roughly 0.3% in the knockdown lines (Figure 1D). These results indicate that RUNDC1 is required for regulated secretion of insulin but not insulin synthesis.

A reduction in stimulated insulin secretion could stem from either a decrease of insulin granules or a defect in granule docking at the plasma membrane. The standard glucose-stimulated insulin secretion protocol involves a 2-hour incubation in basal glucose (2.8 mM), followed immediately by a 1-hour challenge in high glucose (20 mM). To distinguish between a cargo abundance issue and a docking defect, we visualized insulin granules right before stimulation. Specifically, following the 3-day siRNA treatment, we incubated the cells for 2 hours in 2.8 mM glucose and immediately fixed them to examine the localization of the insulin granules.

Under normal glucose conditions, control cells (siCtrl) displayed perinuclear insulin and scattered insulin puncta throughout the cytoplasm (Figure S2). Following a 2-hour incubation in low glucose (2.8 mM), control cells exhibited a striking clearance of this perinuclear insulin pool. This observation is consistent with the repression of *de novo* insulin translation under low glucose conditions, coupled with the ongoing anterograde migration of existing immature granules away from the trans-Golgi network (TGN) and toward the cell periphery (Figure S2). In contrast, RUNDC1KD cells subjected to the same 2-hour low-glucose incubation failed to clear this perinuclear cargo (Figure S2) while there was a noticeable reduction in the density of mature granules lining the plasma membrane compared to controls. This suggests that RUNDC1 knockdown impairs the exit, maturation, or transport of newly budded insulin granules from the TGN area. Consequently, when the cells are subsequently challenged with a high-glucose stimulus, they lack a sufficient pool of docked granules at the plasma membrane, resulting in reduced insulin secretion.

2. RUNDC1 deficiency induces a proinsulin sorting bottleneck and constitutive leakage

Our observation that RUNDC1 knockdown causes insulin granules to accumulate abnormally at the TGN area suggested an issue in early post-Golgi trafficking. Because this occurs at the site where proinsulin, a precursor of insulin, is packaged into immature granules, we reasoned that the insulin trafficking defect might stem from a problem in cargo packaging at the trans-Golgi network, leading us to investigate the abundance and distribution of proinsulin.

In WT and control cells, proinsulin colocalized with TGN38, a marker for the *trans*-Golgi network. However, we found that in *Rundc1*KD cells, while proinsulin seemed to be localized to the right place, there was an excess of proinsulin concentrated near TGN38 (Figure 2A). Fluorescence quantification showed an increase in total proinsulin per cell, which was also confirmed via ELISA (Figure 2A, B). These results suggest that RUNDC1 is a critical factor for the exit of proinsulin from the TGN, and its absence creates a physical bottleneck at the sorting station.

To examine where the extra proinsulin goes, we next considered whether the excess proinsulin is being secreted into the media. Normally, proinsulin secretion is minimal, as most proinsulin is correctly sorted into the regulated secretory pathway for maturation as observed in WT and control cells. Interestingly, knocking down RUNDC1 led to an increase in basal proinsulin secretion (2.8 mM glucose) (Figure 2C). This phenotype suggests a leakage model: because proinsulin cannot efficiently enter the regulated secretory granules due to the lack of RUNDC1, the accumulating precursor overflows into the constitutive secretory pathway, bypassing the normal maturation and storage steps.

Together, these data demonstrate that RUNDC1 is essential for the proper sorting of proinsulin into the regulated pathway at the TGN.

3. RUNDC1 deficiency did not disrupt processing enzymes

Having established that RUNDC1 knockdown leads to a proinsulin bottleneck at the TGN, we sought to determine whether this defect is due to a general failure in the recruitment, or perturbed expression or targeting of processing enzymes.

Proinsulin is processed into mature insulin within the regulatory secretory pathway through a series of sequential proteolytic cleavages. This maturation process is initiated in the TGN and continues within budding immature secretory granules. It begins with

the endoproteolytic cleavage of proinsulin by prohormone convertase 1/3 (PC1/3) and prohormone convertase 2 (PC2), which remove the C-peptide boundaries. Subsequently, carboxypeptidase E (CPE) trims the remaining C-terminal basic residues to generate biologically active, mature insulin. Using immunofluorescence microscopy, we observed that CPE is mainly distributed throughout the cell periphery and partially colocalized with the TGN marker TGN38 in control cells. Notably, knocking down RUNDC1 did not alter this distribution (Figure 3B). Fluorescence quantification also showed that there was no significant difference in the intensity of CPE staining between control and RUNDC1 knockdown conditions.

To better assess cellular protein levels, we performed Western blot analysis for PC1/3, CPE, and proCPE (a precursor or CPE). We found that the protein levels of PC1/3, mature CPE (CPE-N and CPE-C) and its precursor (proCPE) remained unchanged following RUNDC1 knockdown (Figure 3A, C-D). As the delivery of proinsulin processing enzymes remained intact, the observed proinsulin accumulation was not a secondary effect of depleted or mislocalized processing enzymes. These results support that RUNDC1 appears to function as a specific regulator of proinsulin cargo sorting.

4. RUNDC1 is Required for the Kinetic Exit of Newly Synthesized Proinsulin from the TGN

To determine if the TGN accumulation of proinsulin resulted from a transport failure, we monitored cargo trafficking using the (pro)CpepSNAP reporter system. Recently developed by Bearrows et al. (2019) to track nascent proinsulin kinetics, this strategy features a modified proinsulin reporter with an internal SNAP-tag within the C-peptide region.

The SNAP-tag self-labels by covalently binding synthetic benzylguanidine-conjugated probes - a reaction that is irreversible and terminal for each reporter molecule. Taking advantage of this reaction, we were able to selectively isolate and track newly synthesized cargo by first blocking the pre-existing pool using a non-fluorescent SNAP substrate. After a recovery period for *de novo* protein synthesis, cells are pulse-labeled with a cell-permeable, fluorescent TMR-substrate that covalently attaches to the SNAP-tag within the proinsulin C-peptide. As this tagged proinsulin moves from the Trans-Golgi Network (TGN) into maturing secretory granules, it is proteolytically processed into mature insulin and a fluorescent proCpepSNAP fragment. By monitoring the signal during the chase period, we can specifically track the kinetic exit of this "young" cargo, allowing us to visualize the trafficking bottleneck caused by RUNDC1 knockdown.

Following a 2-hour chase, control cells (WT and siCtrl) exhibited a significant distribution of labeled (pro)CpepSNAP throughout the cell periphery, representing cargo that had successfully exited the Golgi (Figure 4B). In contrast, RUNDC1-deficient cells showed a significant reduction in non-TGN fluorescence, with the majority of the labeled signal remaining tightly co-localized with the TGN marker TGN38 (Figure 4B).

By the 3-hour chase interval, we observed that the labeled reporter was eventually able to leave the TGN in RUNDC1-deficient cells (Figure 4C). While the exit was significantly delayed compared to the rapid transit seen in control cells, TMR-labeled (pro)CpepSNAP was not permanently trapped. These results provide kinetic evidence that while RUNDC1 is not strictly required for TGN exit, it is essential for the efficiency and timing of proinsulin export.

2.3 Discussion

Here, we identified RUNDC1 to be an important factor for the regulation of both the sorting and kinetic exit of proinsulin from the trans-Golgi Network (TGN) in insulin-secreting cells. A previous study demonstrated that RUNDC1 homologs are involved in the biogenesis of dense core vesicles (DCVs). However, the exact mechanism through which it functions in mammalian endocrine cells remains undefined.

While we evaluated proinsulin processing by examining the protein levels and localization of prohormone convertase 1/3 (PC1/3) and carboxypeptidase E (CPE), our analysis did not include prohormone convertase 2 (PC2), which also processes proinsulin to insulin. Furthermore, we did not directly measure the enzymatic activity or kinetic cleavage rates of PC1/3 or CPE within the maturing granules. Consequently, these omissions leave open the possibility that while the structural recruitment of these processing enzymes appears intact, their *in vivo* catalytic efficiency may be compromised under RUNDC1KD conditions.

We showed that reducing expression levels of RUNDC1 resulted in a significant decrease in insulin release. We also demonstrated that this reduction was due to a blockage at the level of the TGN and not to defects in post-sorting processing enzymes, including CPE or PC1/3. This sorting defect results in the leakage of unprocessed proinsulin into the constitutive pathway, resulting in elevated basal proinsulin release.

Using a SNAP-tagged pulse-chase system to track real-time movement of newly synthesized cargo, we were able to show that RUNDC1 was required for timely export of young proinsulin from the TGN. Overall, our results illustrate a necessary sorting mechanism to allow for rapid and efficient secretion from the insulin-secreting cell.

A Transient TGN Kinetic Delay Explains the Loss of Acute Glucose-Stimulated Secretion

An interesting outcome from these studies is the dramatic reduction in the ability of RUNDC1-deficient cells to produce and release insulin upon stimulation while having completely normal levels of intracellular insulin. We showed that the expression and maturation of the processing enzymes such as PC1/3 and CPE are fully intact. Hence, we concluded that RUNDC1 is not required for the enzymatic processing of insulin.

We employed a SNAP-tag-based pulse chase experiment and showed that the major problem lies in the speed with which newly made proinsulin leaves the TGN. Newly produced (pro)CpepSNAP cargo leaves the TGN quickly in control cells and reaches the cell surface within two hours. However, in RUNDC1 deficient cells, the young (pro)CpepSNAP cargo is retained at the TGN at the 2-hour chase.

This cargo is not permanently trapped; by 3 hours, the labeled reporter successfully exits the TGN in RUNDC1KD cells. The delayed time in exporting young insulin precursors into the secretory pathway for one hour is enough to cause a significant decrease in glucose-stimulated insulin secretion. β-cells primarily use "young" insulin granules, rather than granules containing older insulin for first phase responses to glucose. Because RUNDC1 acts as a limiting factor to prevent the early release of new insulin-containing vesicles, RUNDC1 deficient cells will not have access to their preferred source of insulin to stimulate them to secrete appropriate amount of insulin in response to glucose.

The Model of Constitutive Proinsulin Leakage

Immunofluorescence images show that knocking down RUNDC1 leads to the accumulation of steady state proinsulin close to the TGN marker TGN38, which indicates that there is a physical blockade in transporting proinsulin. Proinsulin in healthy β-cells is effectively sorted into the regulated secretory pathway, preventing its exposure to the default, constitutive pathway (Arvan and Castle, 1998). The ELISA results showed that RUNDC1 knockdown resulted in significantly increased levels of intracellular proinsulin and basal proinsulin secretion. Since the total amount of insulin stored within cells remained normal, these results provide strong evidence for an “overflow" hypothesis.

We suggest that since proinsulin is unable to be loaded into forming secretory granules due to a lack of RUNDC1, the excess proinsulin at the TGN gate exceeds a physical capacity limit. This excess cargo then goes into constitutive secretory vesicles. These

vesicles are able to bypass normal maturation, storage, and stimulated exocytotic pathways, resulting in increased basal proinsulin being secreted.

Crosstalk with Autophagy Machinery: RUNDC1 as a Coordinate Regulator of Secretory Fidelity

Zhang et al. (2023) demonstrated that RUNDC1 acts as a biochemist to suppress autophagy through promoting ATG14 oligomers and also stabilizes the inactive SNAP29-STX17 intermediate complex that prevents excessive autophagosome-lysosome fusion; therefore, lack of RUNDC1 results in hyperactive autophagic flux. This suggests that RUNDC1 plays a key role in two processes in the β-cell; the regulation of secretory cargo traffic and the suppression of autophagy.

The findings in our study are consistent with the degradation phenotype observed above. Mature insulin containing secretory vesicles have a relatively prolonged physiological half-life of approximately 3 to 5 days (Halban and Wollheim, 1980; Müller et al, 2017); since we evaluated cellular phenotypes after 3 days post siRNA transfection, the existing population of older mature granules remained largely unaffected from prior time points explaining why steady state levels of intracellular insulin appeared normal. However, when exposed to high glucose concentrations, RUNDC1 deficient cells showed diminished GSIS. As previously discussed, the initial phase of the insulin response upon acute glucose stimulation requires the rapid mobilization of "young" pools of proinsulin granules to the readily releasable pool (RRP), located at the plasma membrane. The dynamic movement of these new proinsulin granule pools to the RRP is kinetically delayed due to a blockage at the TGN export gate as evident from our (pro)CpepSNAP pulse-chase data in RUNDC1-deficient cells.

We propose a model that the hyper-active autophagy caused by knockdown of RUNDC1 will cause a "SNARE titration" effect to result in this TGN export delay. Although SNAP29 is a Q-SNARE that does not play a direct role in the budding and/or formation of dense core granules, SNAP29 availability is important for retrograde endosome-to-TGN trafficking pathways required for recycling essential sorting receptor and cargo loading machinery (Rapaport et al, 2010). When RUNDC1 is depleted, the loss of the protective "clasp" on SNAP29 allows hyper-activated autophagic and lysosomal complexes to consume the free SNAP29 pool. There will be no homeostatic recycling machinery available at the TGN to facilitate efficient formation of newly synthesized proinsulin cargo. Thus, RUNDC1 functions as a metabolic gatekeeper, actively suppressing degradative flux to prioritize newly synthesized insulin cargo for acute, nutrient-dependent systemic release.

Pathophysiological Implications for Type 2 Diabetes

The characteristic combination of impaired glucose-stimulated insulin release along with increased levels of circulating proinsulin-to-insulin are hallmarks of β-cell decompensation observed in patients with Type 2 Diabetes (T2D). This was previously referred to as hyperproinsulinemia and thought to be primarily caused by reduced amounts of secretory vesicles (dense core granules) or defective enzymes involved in the processing of proinsulin (PC1/3 and CPE).

Here, we show that defects in early-stage cellular trafficking apparatus can cause similar clinical phenotypes. RUNDC1 deficient cells contain intact processing enzymes (PC1/3 and CPE) but have a severely blunted glucose stimulated insulin secretion (GSIS) response coupled with significant proinsulin leakage due to a kinetic bottleneck located at the TGN.

Hence, it's likely that downregulation of TGN sorting machinery, similar to RUNDC1, may play a direct role in contributing to the pathophysiology of β-cell dysfunction in T2D. Thus, understanding the molecular pathways which regulate RUNDC1 expression and function during periods of metabolic stress provides a new and exciting area for identification of potential therapeutic targets for restoration of normal insulin production in diabetes.

2.4 Materials and Methods

Cell culture

The INS-1-derived 832/13 cell line was originally isolated by Dr. Christopher Newgard (Duke University School of Medicine) and provided by Dr. Duk-Su Koh via Dr. Ian Sweet (both from the University of Washington). For experiments involving RUNDC1, 832/13 cell lines were used for most experiments (except the (pro)CpepSNAP experiments). All 832/13 and derivative lines were maintained in RPMI 1640-GlutaMAX (GIBCO) supplemented with 10% FBS (RMBIO), 10 mM HEPES (GIBCO), 1 mM sodium pyruvate (GIBCO), and 0.0005% beta-mercaptoethanol.

The (pro)CpepSNAP line (an INS-1-derived 832/3 line) was a gift from Dr. Samuel Stephens (University of Iowa).

Generation of RUNDC1 knockdown (KD) cells

To generate RUNDC1KD cells, 832/13 cells were seeded in 6-well plates and grown to 50 - 60% confluency. Cells were transfected with two distinct predesigned siRNAs (30

nM/well, Sigma-Aldrich) targeting rat *Rundc1* using Lipofectamine 2000 (Thermo Fisher Scientific) according to the manufacturer's instructions.

Experimental groups were compared against cells transfected with a non-targeting siRNA control duplex or wild-type cells. The siRNA sequences used were as follows:

siRUNDC1_1: ACCGCACGUUCCGCACGCUG

siRUNDC1_2: CACUGUGAGUGCAAGACCAG

After 72 hours, cells were harvested, and knockdown efficiency was validated via RT-qPCR.

RNA extraction and RT-qPCR

Total RNA was extracted from WT, siCtrl, and siRUNDC1 treated cells using TRIzol (Invitrogen) and subjected to reverse transcription quantitative PCR (RT-qPCR) according to manufacturer's protocol. 1 µg of RNA was collected for cDNA synthesis using the QuantiTekt Reverse Transcription kit (Qiagen).

iTaq Universal SYBR Green Supermix (Bio-rad) was used according to manufacturer's instructions. RUNDC1 mRNA expression levels were detected using the CFX Opus 96 (Bio-rad), normalized against GAPDH or cyclophilin A mRNA levels. mRNA abundance was calculated using the ΔΔCt method (Hellemans et al., 2007). The primers utilized for the detection of RUNDC1 cDNA were:

- Forward Primer: AGAGCAGTTAGTGGAACAGCTG
- Reverse Primer: CGCTGGTCTTGCACTCACAG

Immunofluorescence

INS-1 832/13 cells were plated onto poly-Lysine coated coverslips (Thomas Scientific #121N79) in 6-well plates. After 24-hour incubation, RUNDC1 knockdown was induced by transfection of siRNAs when indicated. For RUNDC1::GFP construct, cells were transfected with 2ug of purified plasmid using Lipofectamine 2000 (Thermo Fisher) 24-48 hours post cell seeding.

After 24 hours of transfection with plasmid or 72 hours of siRNA treatment, cells were gently rinsed twice with PBS, fixed with 4% paraformaldehyde (in PBS) for 20 minutes and permeabilized in 0.5% Triton X-100 (in PBS). After blocking in 5% milk (in PBS) for 1 hour, cells were incubated in primary antibodies solution (0.5% milk in PBS) against proteins of interest for another 1 hour. Cells were then incubated with highly cross-adsorbed Alexa Fluor-conjugated secondary antibodies (Invitrogen) for 1 hour and

mounted using Gelvatol medium. Three PBS washes are done after fixation, permeabilization, blocking, and antibodies incubation. All steps were carried at room temperature. All solutions were made fresh from stock on the day of the experiment.

All images were obtained using a spinning disk Nikon ECLIPSE Ti2.

SNAP-tag Pulse Chase Labeling

To temporally resolve the trafficking of newly synthesized proinsulin, we employed an *in situ* pulse-chase fluorescent labeling strategy in 832/3 cells stably expressing proCpepSNAP. The INS-1 832/13 and 832/3 lines are both human proinsulin-transfected subclones of the parental INS-1 rat insulinoma line, engineered for their robust glucose-stimulated insulin secretion (GSIS). We used 832/13 in other experiments as it exhibited a more robust glucose response. The proCpepSNAP cells were engineered using 832/3 cell line by Samuel Stephens lab.

ProCpepSNAP cells were plated on HTB9-coated coverslips 48 hours post-siRNA transfection (siCtrl or siRUNDC1) and cultured overnight. The labeling procedure was initiated by incubating cells with SNAP-cell Block (10 μM; NEB) for 20 minutes to mask the existing pool of proCpepSNAP. Following three 10-minute washes, cells were cultured for an additional 2 hours to allow for the *de novo* synthesis of unlabeled reporter. For the pulse-labeling phase, cells were incubated with SNAP-cell-TMR (1 μM; NEB) for 20 minutes, followed by three 10-minute washes in culture media with reduced glucose (5 mM). Cells were then chased for the indicated times (0, 2 or 3 hours) and fixed in 4% formaldehyde.

Fixed cells were stained with primary antibodies against insulin, and TGN38, which were detected using appropriate Alexa Fluor-conjugated secondary antibodies (Invitrogen).

Images were captured using a spinning disk Nikon ECLIPSE Ti2.

Insulin/proinsulin secretion assays and ELISA

Glucose stimulated proinsulin/insulin secretion was measured in INS-1 832/13 cells. Cells were seeded in 24-well plates and grown to near confluency. Glucose-free Krebs-Ringer Bicarbonate Buffer (KRBB) (110.8 mM NaCl, 4.87 mM KCl, 2.29 mM $CaCl_2 \cdot 2H_2O$, 1.22 mM KH_2PO_4, 1.21 mM $MgSO_4 \cdot 7H_2O$, 25.7 mM $NaHCO_3$, 10.4 mM HEPES, and 0.2% BSA) was supplemented with the appropriate glucose to reach the desired glucose concentration in the final solution. Cells were washed three times in 2.8mM glucose KRBB and pre-incubated in KRBB containing 2.8 mM glucose (basal)

for 1 h at 37°C. Following pre-incubation, cells were incubated in KRBB containing either 2.8 mM or 20 mM glucose (stimulatory) for 1 h.

Secreted proinsulin and insulin were measured from the supernatant using the commercially avaialble rat proinsulin ELISA (Mercodia) and rat insulin ELISA (Alpco) respectively. For measurement of total insulin content, cells were lysed overnight at -20°C in 0.44M HCl/95% ethanol.

All secretion data were normalized to total protein concentration (determined via BCA assay) or cell numbers.

SDS-PAGE and Western Blotting

To quantify the steady-state protein levels of proinsulin-processing enzymes, cell lysates were prepared from WT, siCtrl, and siRUNDC1 treated cells. Protein extracts were resolved on 10% SDS-PAGE gels and transferred onto PVDF membranes.

For the analysis of CPE, proCPE, and CPD, membranes were blocked using 5% milk solution for 1 hour at room temperature. Membranes were subsequently incubated overnight at 4°C with specific primary antisera (generous gifts from Dr. Lloyd Fricker) diluted in 5% milk solution supplemented with 0.2% Tween 20:

- **Anti-CPE-N terminus:** An antiserum raised against the N-terminal 15 amino acids of bovine CPE (Fricker et al., 1990).
- **Anti-pro-CPE:** An antiserum generated against a synthetic 12-residue peptide (QEPGAPAAMGRR) corresponding to the pro-region of mouse, rat, and human pro-CPE, synthesized with an additional C-terminal cysteine residue (QEPGAPAAMGRRC) to facilitate conjugation to maleimide-activated keyhole limpet hemocyanin (KLH) carrier protein.
- **Anti-CPE-C terminus:** An antiserum raised against a 9-residue synthetic peptide (KMMSETLNF) corresponding to the extreme C-terminus of mouse CPE (Fricker et al., 1996).

Following three 5-minute washes with PBST (PBS + 0.1% Tween 20), membranes were incubated for 1 hour at room temperature with appropriate secondary antibodies diluted in 5% milk solution supplemented with 0.2% Tween 20.

Blots were imaged using a LI-COR Odyssey CLx imaging system.

Statistics

Data are presented as the mean ± SEM. Statistical significance was determined using a one-way ANOVA for comparisons between two groups. For experiments involving multiple variables—such as GSIS—a two-way ANOVA followed by Sidak's post-hoc test was performed for multiple group comparisons. All statistical analyses were conducted using GraphPad Prism, and a p-value of < 0.05 was considered statistically significant.

2.5 Acknowledgement

We thank Amy Clippinger, Alex Nam, Lews Caro, Irini Topalidou, Michael Crawford, Alexey Merz, Jihong Bai, Suzanne Hoppins, Sandra Bajjalieh, Sakeneh Zraika and members of the Diabetes Research Center (University of Washington) for their technical help and input throughout this project. We thank Alexey Merz and Jihong Bai for their comments on the manuscript, Christopher Newgard, Ian Sweet, and Duk-Su Koh for the 832/13 cells, Samuel Stephens for the (pro)CpepSNAP 832/3 cells.

2.6 Figures

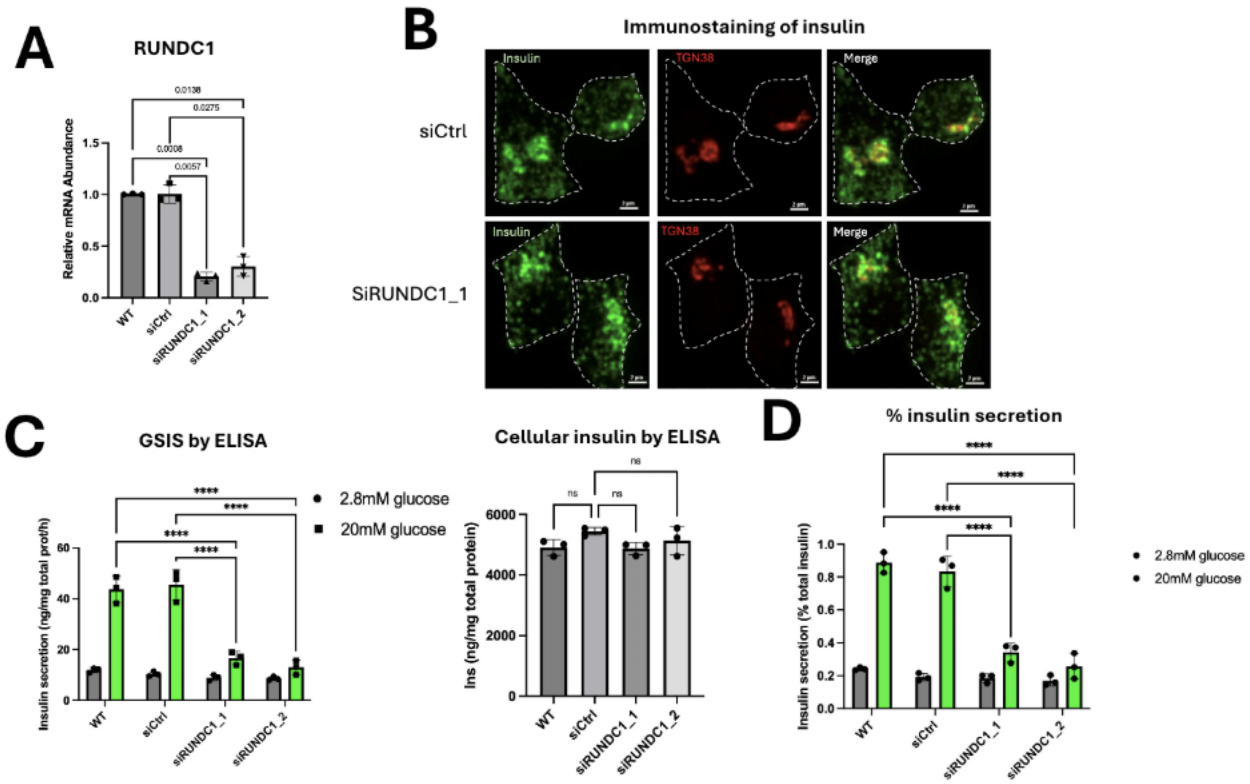

Figure 1. RUNDC1 is required for glucose-stimulated insulin secretion in beta-cells

A. Quantitative PCR (qPCR) analysis of RUNDC1 mRNA level in INS-1 832/13 cells treated with non-targeting control siRNA (siCtrl) or two independent RUNDC1-targeting siRNAs. n = 3 each, one-way ANOVA with Tukey's multiple comparison.

B. Representative confocal immunofluorescence images showing the intracellular distribution of insulin in control and RUNDC1-deficient cells. INS-1 derived cells (832/13) were fixed and immunostained for Insulin (green) and the trans-Golgi network marker TGN38 (red). Scale bars: 2 μm. Cell boundaries are indicated by white dashed lines.

C. Insulin secretion was measured via ELISA in cells incubated in basal (2.8 mM) or stimulatory (20 mM) glucose concentrations for 1 hour. RUNDC1 knockdown severely eliminated glucose-stimulated insulin secretion (GSIS) compared to control groups. n = 3 each, two-way ANOVA with Šidák's multiple comparison (left panel).

Total cellular insulin content was measured by ELISA in cell lysates. No significant difference in total insulin abundance was observed between WT, siCtrl, and RUNDC1

knockdown cells. n = 3 each, one-way ANOVA with Tukey's multiple comparison (right panel).

D. Secreted insulin expressed as a percentage of total insulin content. Knockdown of RUNDC1 results in a marked decrease in the fractional release of insulin in response to glucose stimulation. n = 3 each, two-way ANOVA with Šidák's multiple comparison.

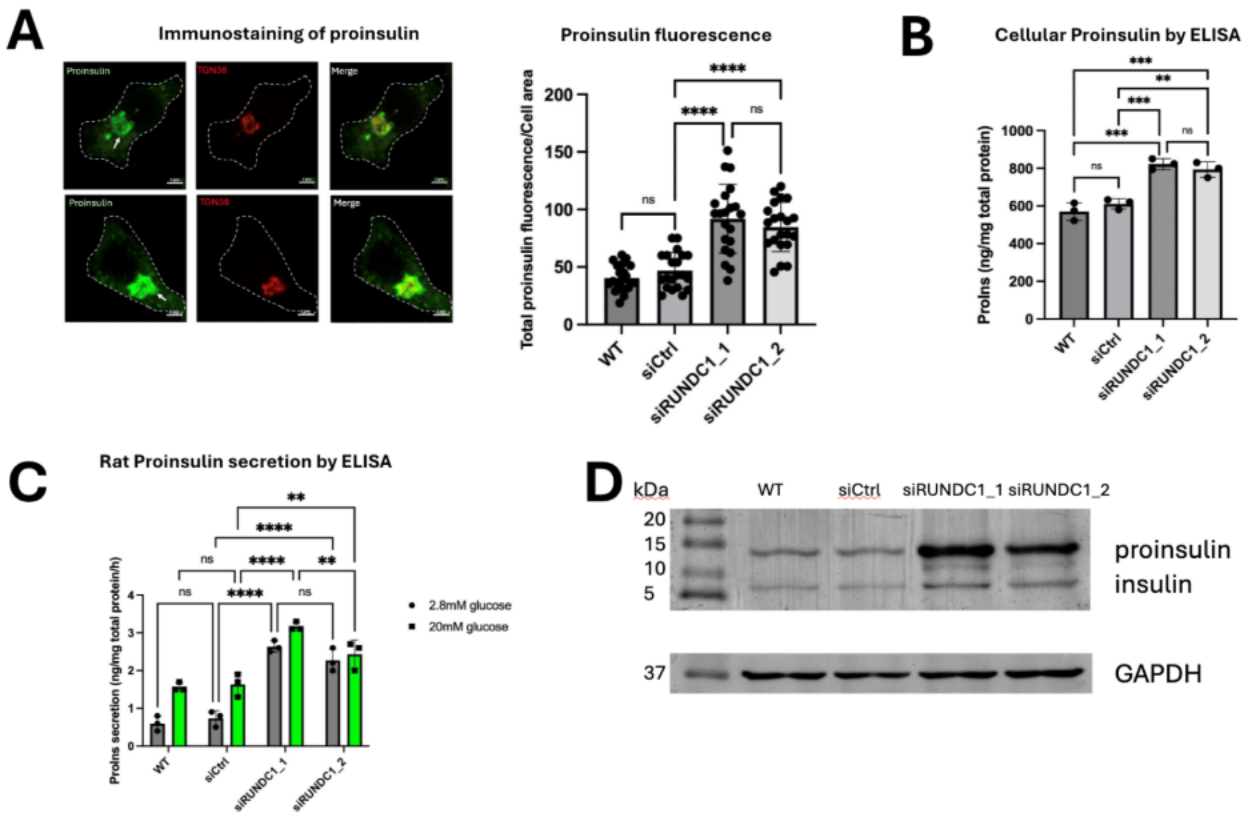

Figure 2. RUNDC1 is critical for the proper maturation and trafficking of proinsulin

A. Immunofluorescence (IF) microscopy of proinsulin (green) and the TGN marker TGN38 (red) in control and RUNDC1-deficient cells. In RUNDC1 KD cells, proinsulin exhibits a distinct accumulation near the Golgi region (white arrows) (left panel).

Quantification of total cellular proinsulin fluorescence intensity per cell area. Data points represent individual cells, showing a significant increase in proinsulin abundance following RUNDC1 knockdown compared to WT and siCtrl groups (right panel), n = 21, two-way ANOVA with Šidák's multiple comparison.

B. Total cellular proinsulin content was measured by ELISA in INS-1 832/13 cell lysates. siRUNDC11 and siRUNDC1_2 resulted in a marked accumulation of intracellular proinsulin compared to WT and siCtrl groups, n = 3, two-way ANOVA with Šidák's multiple comparison.

C. Proinsulin secretion was measured via ELISA under basal (2.8 mM) and stimulatory (20 mM) glucose conditions. RUNDC1-deficient cells exhibited elevated basal proinsulin release and an overall increase in secreted proinsulin compared to controls, suggesting a bypass of the regulated secretory pathway, n = 3, two-way ANOVA with Šidák's multiple comparison.

D. Representative Western blot analysis of using a pan-insulin antibody that recognizes both proinsulin and insulin. Cells were left untreated (WT), transfected with a non-targeting control siRNA (siCtrl), or transfected with two independent siRNAs targeting RUNDC1 (siRUNDC1_1 and siRUNDC1_2) for 3 days. Molecular weight markers (kDa) are indicated on the left. GAPDH was used as a loading control to ensure equal protein loading across all lanes.

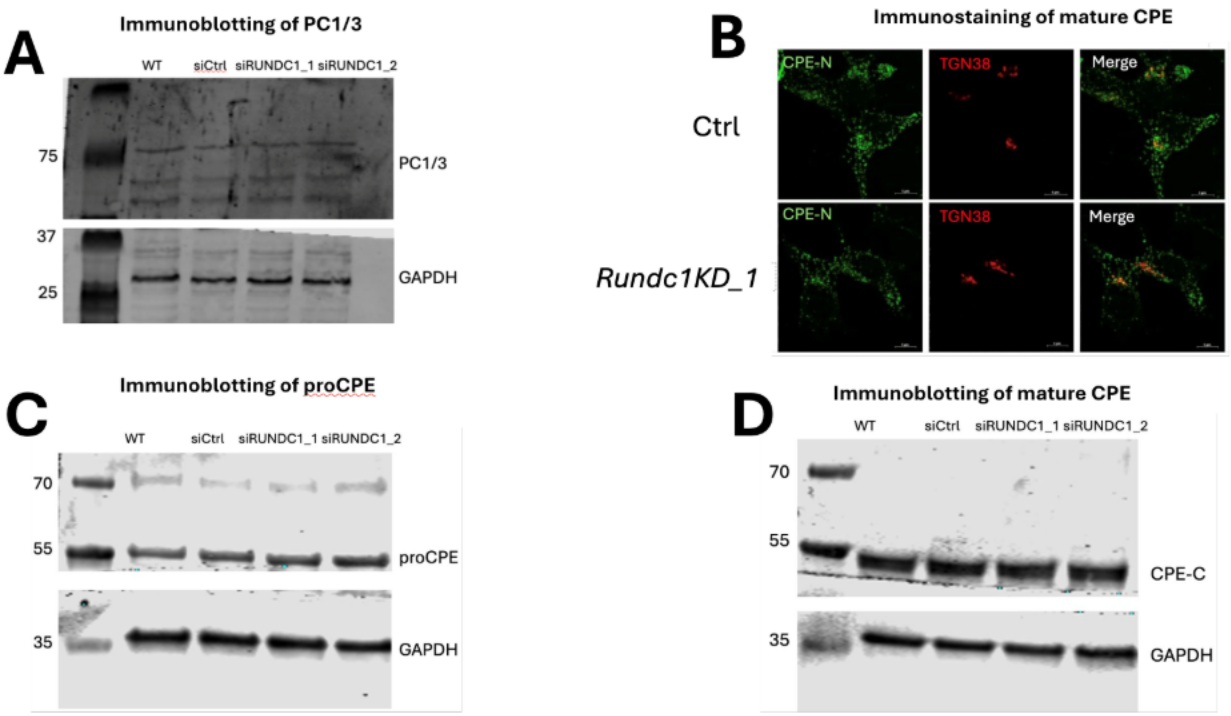

Figure 3. RUNDC1 knockdown does not impair the localization or expression of proinsulin-processing enzymes

A. Representative Western blot analysis of intracellular prohormone convertase 1/3 (PC1/3) levels in INS-1 cells. Lysates were prepared from untreated cells (WT), cells transfected with a non-targeting control siRNA (siCtrl), or cells transfected with two independent siRNAs targeting RUNDC1 (siRUNDC1_1 and siRUNDC1_2) for 3 days. The PC1/3 antibody recognizes multiple molecular weight forms corresponding to the pro-enzyme and cleaved, mature variants of the protease. GAPDH was used as a loading control to verify equal protein loading across lanes.

B. Immunofluorescence (IF) microscopy of 832/13 cells transfected with control siRNA (siCtrl) or RUNDC1-targeted siRNA, co-stained for Carboxypeptidase E (CPE, green) and the trans-Golgi network marker TGN38 (red). RUNDC1KD cells exhibit a normal, punctate distribution of CPE, with no observable alteration in overall cellular localization compared to control cells.

C-D. WB analysis of steady-state protein levels for mature CPE (CPE-N, CPE-C) and its precursor (proCPE). No significant changes in expression levels were observed between Ctrl and RUNDC1 KD cells, demonstrating that the proinsulin maturation defect is not caused by a depletion of essential processing machinery.

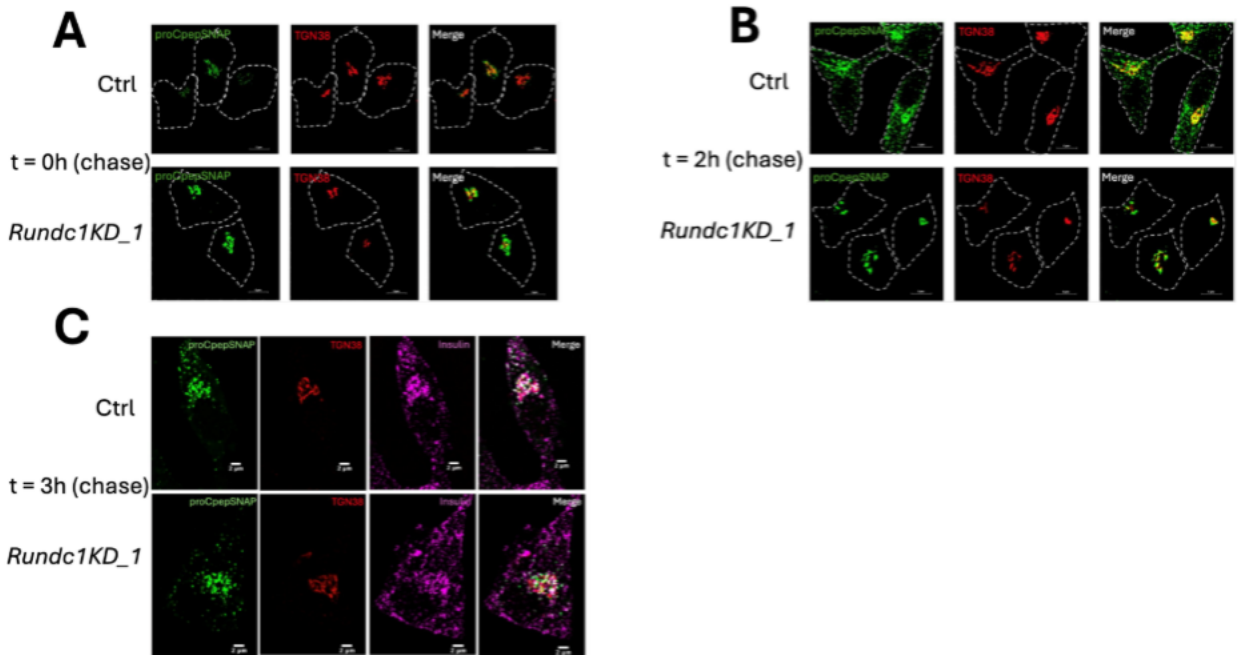

Figure 4. RUNDC1 is required for the exit of newly synthesized proinsulin from the TGN

A. INS-1 832/3 cells stably expressed a proCpepSNAP reporter and pulse-labeled to track the temporal movement of newly synthesized proinsulin. Representative images at t = 0h chase show (pro)CpepSNAP (green) localied with the TGN marker TGN38 (red) in both control and RUNDC1KD cells.

B. Representative images at t = 2h chase show (pro)CpepSNAP (green) is trapped with the TGN marker TGN38 (red) in Rundc1KD cells.

C. Prolonged TGN retention at t = 3h chase. Triple-staining of mature insulin (green), proCpepSNAP (red), and TGN38 (magenta) at 3 hours post-labeling. (pro)CpepSNAP signal is dispersed, co-localizing with mature insulin-positive secretory granules at the cell periphery in KD cells.

SUPPLEMENTAL MATERIALS

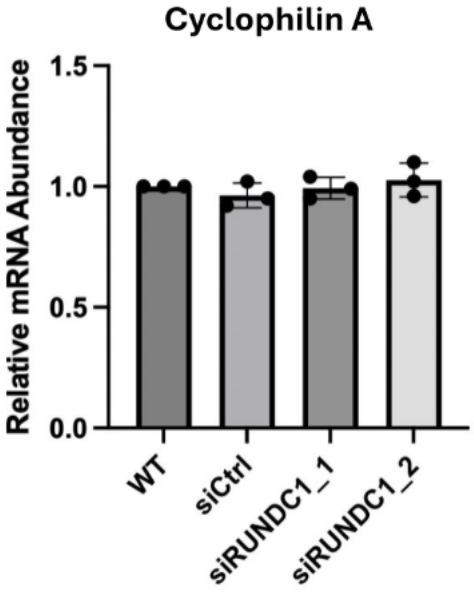

Figure S1. Quantitative RT-PCR analysis of Cyclophilin A mRNA. RNA was isolated 3 days post-transfection from untreated cells (WT), cells transfected with a non-targeting control siRNA (siCtrl), or cells transfected with two independent siRNAs targeting RUNDC1 (siRUNDC1_1 and siRUNDC1_2). Data are presented as mean relative mRNA abundance ± SEM, n = 3, two-way ANOVA with Šidák's multiple comparison.

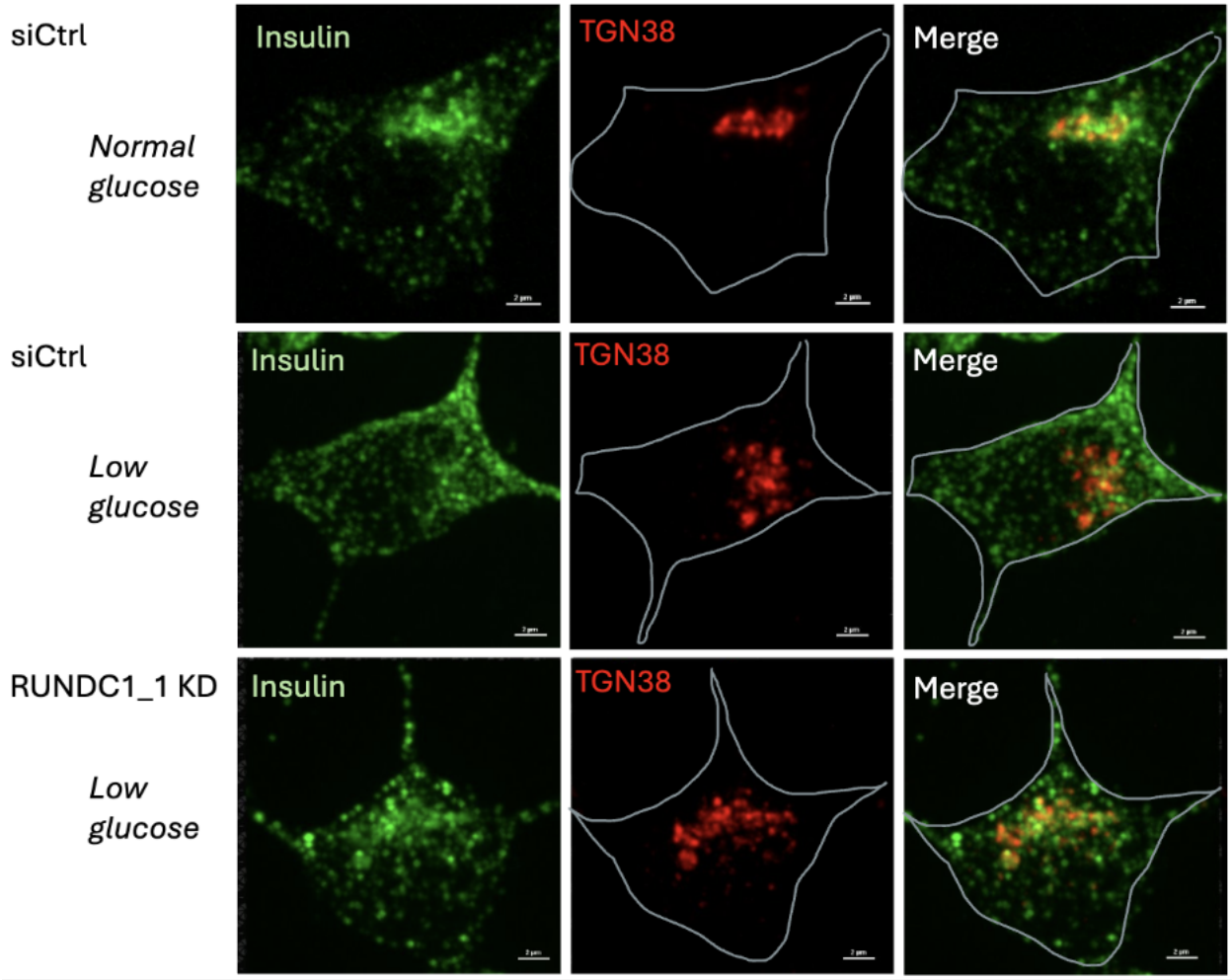

Figure S2. Representative immunofluorescence images showing the subcellular localization of insulin (green) and the trans-Golgi network marker TGN38 (red). Under normal glucose conditions, control cells (siCtrl) display insulin cluster at the perinuclear region co-localizing with TGN38, alongside peripheral puncta distributed throughout the cytosol (top panel). Following a 2-hour incubation in low glucose (2.8 mM), control cells exhibit a substantial clearance of the perinuclear insulin pool, with mature granules lining the plasma membrane (middle panel). In contrast, RUNDC1 knockdown cells (RUNDC1_1 KD) fail to clear insulin from the TGN area under low glucose conditions, showing mainly perinuclear insulin localization (bottom panel). White solid lines demarcate cell boundaries. Scale bars: 2 um.

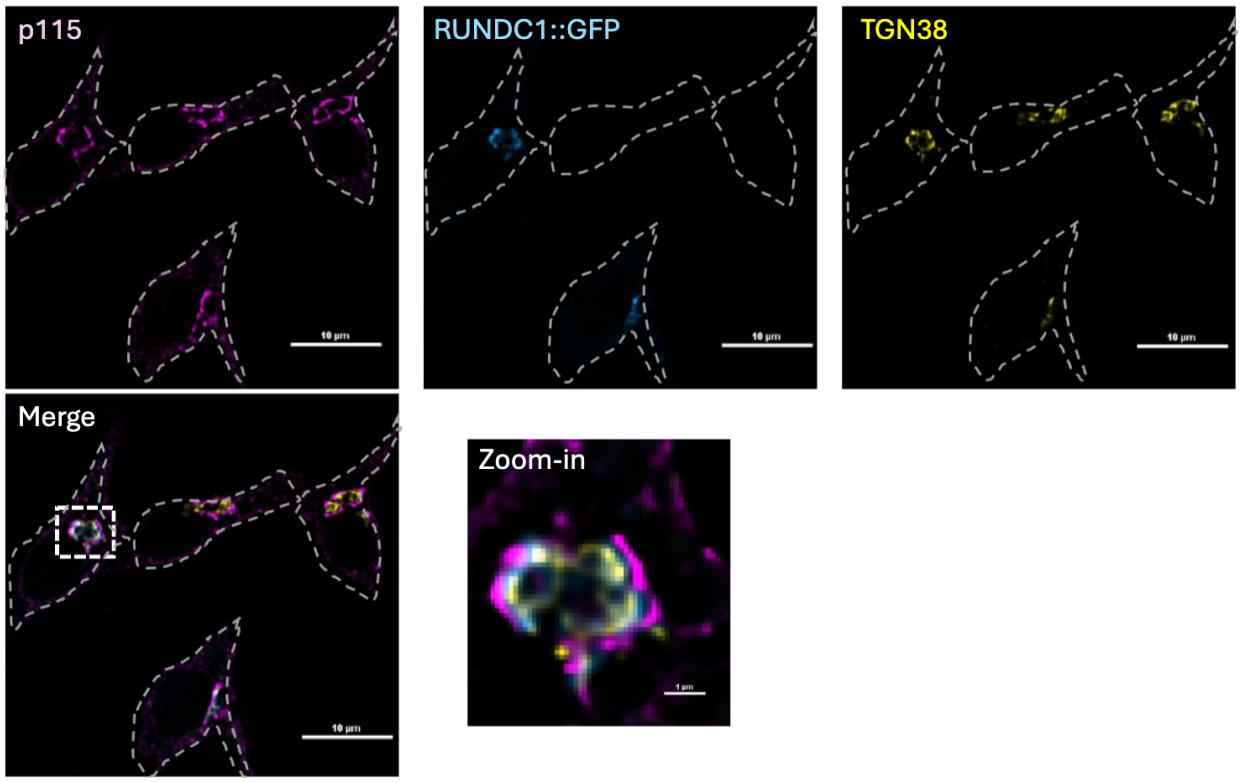

Figure S3. Representative confocal immunofluorescence image displaying the localization of RUNDC1-GFP in 832/13 cells. Cells are immunostained for the *cis*-Golgi matrix protein p115 (magenta) and the *trans*-Golgi network (TGN) resident marker TGN38 (yellow), alongside direct fluorescence detection of RUNDC1-GFP (pseudo color to cyan). Dashed white lines delineate individual cell boundaries.

REFERENCES

Bearrows, Shelby C., et al. "Chromogranin B Regulates Early-Stage Insulin Granule Trafficking from the Golgi in Pancreatic Islet β-Cells." *Journal of Cell Science*, vol. 132, no. 13, 2019, https://doi.org/10.1242/jcs231373.

Chen, Y. C., et al. "Deletion of Carboxypeptidase E in β-Cells Disrupts Proinsulin Processing but Does Not Lead to Spontaneous Development of Diabetes in Mice." *Diabetes*, vol. 72, no. 9, 2023, pp. 1277–88, https://doi.org/10.2337/db22-0945.

Daniel, S., et al. "Identification of the Docked Granule Pool Responsible for the First Phase of Glucose-Stimulated Insulin Secretion." *Diabetes*, vol. 48, no. 9, 1999, pp. 1686–90.

Fricker, L. D., et al. "Identification of the pH-Dependent Membrane Anchor of Carboxypeptidase E (EC 3.4.17.10)." *The Journal of Biological Chemistry*, vol. 265, no. 5, 1990, pp. 2476–82.

Fricker, L. D., et al. "Carboxypeptidase E Activity Is Deficient in Mice with the Fat Mutation: Effect on Peptide Processing." *The Journal of Biological Chemistry*, vol. 271, no. 48, 1996, pp. 30619–24.

Gold, G., et al. "Heterogeneity and Compartmental Properties of Insulin Storage and Secretion in Rat Islets." *The Journal of Clinical Investigation*, vol. 69, no. 3, 1982, pp. 519–26, https://doi.org/10.1172/JCI110481.

Halban, P. A., and C. B. Wollheim. "Intracellular Degradation of Insulin Stores by Rat Pancreatic Islets in Vitro: An Alternative Pathway for Homeostasis of Pancreatic Insulin Content." *Journal of Biological Chemistry*, vol. 255, no. 13, 1980, pp. 6003–06.

Halban, Philip A., et al. "β-Cell Failure in Type 2 Diabetes: Postulated Mechanisms and Prospects for Prevention and Treatment." *The Journal of Clinical Endocrinology & Metabolism*, vol. 99, no. 6, 2014, pp. 1983–92, https://doi.org/10.1210/jc.2014-1425.

Ivanova, Anna, et al. "Age-Dependent Labeling and Imaging of Insulin Secretory Granules." *Diabetes*, vol. 62, no. 11, 2013, pp. 3687–96, https://doi.org/10.2337/db12-1819.

Jackson, R. S., et al. "Obesity and Impaired Prohormone Processing Associated with Mutations in the Human Prohormone Convertase 1 Gene." *Nature Genetics*, vol. 16, no. 3, 1997, pp. 303–06, https://doi.org/10.1038/ng0797-303.

Müller, A., et al. "A Global Approach for Quantitative Super Resolution and Electron Microscopy on Cryo and Epoxy Sections Using Self-Labeling Protein Tags." *Scientific Reports*, vol. 7, no. 1, 2017, p. 23, https://doi.org/10.1038/s41598-017-00033-x.

Naggert, J. K., et al. "Hyperproinsulinaemia in Obese Fat/Fat Mice Associated with a Carboxypeptidase E Mutation Which Reduces Enzyme Activity." *Nature Genetics*, vol. 10, no. 2, 1995, pp. 135–42, https://doi.org/10.1038/ng0695-135.

Olofsson, Charlotta S., et al. "Fast Insulin Secretion Reflects Exocytosis of Docked Granules in Mouse Pancreatic B-Cells." *Pflügers Archiv - European Journal of Physiology*, vol. 444, no. 1-2, 2002, pp. 43–51, https://doi.org/10.1007/s00424-002-0814-1.

Orci, L. "Macro- and Micro-Domains in the Endocrine Pancreas." *Diabetes*, vol. 31, no. 6, 1982, pp. 538–65.

Orci, L., M. Ravazzola, and A. Perrelet. "(Pro)insulin Associates with Golgi Membranes of Pancreatic B Cells." *Proceedings of the National Academy of Sciences*, vol. 81, no. 21, 1984, pp. 6743–46, https://doi.org/10.1073/pnas.81.21.6743.

Qin, Ting, et al. "Munc18b Increases Insulin Granule Fusion, Restoring Deficient Insulin Secretion in Type-2 Diabetes Human and Goto-Kakizaki Rat Islets with Improvement in Glucose Homeostasis." *EBioMedicine*, vol. 16, 2017, pp. 262–74, https://doi.org/10.1016/j.ebiom.2017.01.030.

Rapaport, Dorit, Yoav Lugassy, and Eli Sprecher. "Loss of SNAP29 Impairs Endocytic Recycling and Cell Motility." *PLoS ONE*, vol. 5, no. 3, 2010, p. e9759, https://doi.org/10.1371/journal.pone.00009759.

Zhang, R., et al. "RUNDC1 Inhibits Autolysosome Formation and Survival of Zebrafish via Clasping ATG14-STX17-SNAP29 Complex." *Cell Death & Differentiation*, vol. 30, no. 10, 2023, pp. 2231–48, https://doi.org/10.1038/s41418-023-01215-z.

Zhu, D., et al. "Dual Role of VAMP8 in Regulating Insulin Exocytosis and Islet β Cell Growth." *Cell Metabolism*, vol. 16, no. 2, 2012, pp. 238–49, https://doi.org/10.1016/j.cmet.2012.07.001.

Zhu, D., et al. "Munc18c Mediates Exocytosis of Pre-Docked and Newcomer Insulin Granules Underlying Biphasic Glucose Stimulated Insulin Secretion in Human Pancreatic Beta-Cells." *Molecular Metabolism*, vol. 4, no. 5, 2015, pp. 418–26, https://doi.org/10.1016/j.molmet.2015.02.004.

CHAPTER 3

BIOCHEMICAL REGULATION OF THE RAB-2 GTPASE CYCLE BY RUND-1 AND TBC-8

Introduction

The regulated secretion of hormones, neurotransmitters, and enzymes is a fundamental process in eukaryotic physiology, requiring the biogenesis of secretory granules (SGs). This process begins at the trans-Golgi network (TGN), where specialized cargo must be sorted away from constitutive secretory pathways and packaged into budding vesicles (Caro and Palade, 1964; Jamieson and Palade, 1967). The fidelity of this sorting mechanism is important; however, the molecular coordination between the budding machinery at the TGN and the maturation of post-Golgi SGs remains a central question in cell biology.

Members of the Rab family of small GTPases function as pivotal molecular switches that govern every stage of vesicular trafficking (Sumakovic et al, 2009; Edwards et al, 2009; Cazares et al, 2014; Neuman et al, 2021). Among these, RAB-2 has been characterized as a master regulator of SG maturation. In *Caenorhabditis elegans*, RAB-2 activity is essential for the proper retention of luminal and transmembrane cargoes (Sumakovic et al, 2009; Edwards et al, 2009). A critical feature of RAB-2-mediated regulation is the requirement for precise GTPase cycling. Previous genetic studies have demonstrated that both GTP-locked (constitutively active) and GDP-locked (dominant negative) RAB-2 variants result in profound cargo-sorting defects that phenocopy null mutations (Sumakovic et al, 2009). These observations suggest that the biological function of RAB-2 is not merely dependent on its "on" state, but rather on the spatiotemporal precision of its activation and subsequent inactivation.

The inactivation of Rab GTPases is catalyzed by GTPase-activating proteins (GAPs), which accelerate the low intrinsic rate of GTP hydrolysis (Pan et al, 2006; Nickerson et al, 2012; Pfeffer, 2017). TBC-8 has been identified via genetic and yeast two-hybrid screens as a putative GAP for RAB-2 (Hannemann et al, 2012). Interestingly, forward genetic screens in *C. elegans* for SG-defective mutants also identified RUND-1, a RUN-domain-containing protein that interacts with both the active form of RAB-2 and its regulator, TBC-8 (Ailion et al, 2014).

Loss-of-function mutations in *rab-2*, *rund-1*, or *tbc-8* lead to decreased secretory cargos, where secretory granules are morphologically normal but fail to retain their specialized cargo. This genetic evidence, coupled with the colocalization of these factors at the TGN in both worms and insulin-secreting cells, suggests that they function at the same step in secretory granule biogenesis (Sumakovic et al, 2009; Edwards et al, 2009;

Hannemann et al, 2012; Ailion et al, 2014; Matsunaga et al, 2016). However, it remains unknown whether RUND-1 functions as a conventional effector for RAB-2 signaling or as a regulatory scaffold that modulates TBC-8-mediated hydrolysis.

While TBC-8 is predicted to be a GAP based on its conserved TBC (Tre2/Bub2/Cdc16) domain, its catalytic activity toward RAB-2 has not been directly demonstrated *in vitro* (Hannemann et al, 2012). In the present study, we utilize purified recombinant proteins to provide the first biochemical confirmation of TBC-8's GAP activity. We demonstrate that RUND-1 acts as a potent negative regulator of TBC-8-mediated hydrolysis. Our findings establish a biochemical model for RAB-2 regulation, wherein RUND-1 coordinates the longevity of the active GTPase state to ensure efficient cargo sorting during secretory granule biogenesis.

Result

TBC-8 is a GAP for RAB-2 and is regulated by RUND-1

To investigate the biochemical regulation of the RAB-2 GTPase cycle, we purified GST-RAB-2, RUND-1, and MBP-TBC-8. Purified GST-RAB-2 predominantly formed homodimers (99kDa), as expected due to the dimeric nature of the GST tag (Fig. S1A, C). RUND-1 existed in a monomer-dimer equilibrium, with peaks observed at 67kDa and 138kDa (Fig. S1A, B). Upon pre-loading GST-RAB-2 with GTP and subsequently mixing it with RUND-1, we observed a significant shift in mass distribution, with the appearance of distinct species at 120 kDa and 250 kDa (Fig. S1D). These shifts indicate the formation of stable heteromeric complexes between RAB-2 and RUND-1. These data demonstrate a direct physical interaction between the GTP-bound, active form of the GTPase and the RUND-1, agreeing with previous yeast two-hybrid findings indicating that RUND-1 preferentially interacts with GTP-bound RAB-2 (Ailion et al., 2014). Hence, our purified proteins are biochemically functional and capable of recapitulating known interactions *in vitro*.

Full-length TBC-8 has been challenging to purify. We attempted to purify MBP-TBC-8 and were able to collect minimal protein elution with high degradation products (Figure 2S). While an immunoreactive band corresponding to the expected molecular weight of full-length MBP-TBC-8 was detected, both fractions exhibited other lower molecular weight degradation products, indicating proteolytic instability during expression or purification. Because mass photometry requires homogenous sample profiles to accurately resolve macromolecular assemblies, the presence of these prominent degradation species prevented the use of intact MBP-TBC-8 in mass photometer analyses. The MBP tag was proteolytically cleaved prior to evaluating TBC-8 in downstream GTP hydrolysis assays.

We first performed in vitro GTPase assays using purified full-length proteins. Using a malachite green colorimetric assay to monitor the release of inorganic phosphate (P_i), we observed that RAB-2 exhibits low intrinsic GTP hydrolysis activity. However, the addition of TBC-8 resulted in a robust, concentration-dependent increase in P_i release, identifying TBC-8 as a potent GTPase-activating protein (GAP) for RAB-2 (Fig. 1A).

We previously identified RUND-1 as a potential interactor with RAB-2 and TBC-8 (Ailion et al, 2014). To test its effect on TBC-8 activity, we added RUND-1 into the GAP assay. Interestingly, the addition of 1uM RUND-1 significantly suppressed TBC-8-mediated GTP hydrolysis (Fig. 1A). This inhibition was dose-dependent, with increasing concentrations of RUND-1 leading to a linear decrease in TBC-8 GAP activity (Fig. 1B). Because TBC-8 functions to transition RAB-2 from its active GTP-bound state to its inactive GDP-bound state, these results suggest that RUND-1 acts to oppose this inactivation. Rather than acting as a simple inhibitor of the pathway, RUND-1 likely serves to prolong or stabilize the active, GTP-bound state of RAB-2.

The TBC domain of TBC-8 is sufficient for RAB-2 GAP activity

While full-length TBC-8 is a functional GAP, its purification as an MBP-fusion was challenging. To define the minimal catalytic unit, we generated a truncation containing only the TBC domain (residues 568–913) (Fig. 2A). Following His6-SUMO cleavage, the untagged TBC domain was collected (Fig. 2B). To bypass the dimerization artifact caused by the GST tag used in previous assays, we also purified a monomeric RAB-2 construct (RAB-2-His8).

We used Mass Photometry to verify the interaction between the isolated TBC domain and RAB-2. The TBC domain alone was confirmed to be a monomer in solution (49kDa peak) (Fig. S3A). When mixed with RAB-2-His_8, the population shifted to a single peak at 65kDa, which corresponds to the predicted mass of a 1:1 TBC:RAB-2 heterodimer (Fig. S3B). These data demonstrate that the TBC domain is both structurally and functionally sufficient for RAB-2 binding and catalysis.

In vitro GTP hydrolysis assays were performed using a malachite green colorimetric assay to monitor the release of P_i across an increasing concentration gradient of the isolated TBC-8 TBC domain against a fixed 6uM active, GTP-loaded RAB-2. In canonical TBC-domain GAP proteins, a highly conserved "arginine finger" within the catalytic motif is structurally required to stabilize the transition state of the target Rab GTPase. The wild-type TBC domain demonstrated a dose-dependent increase in released P_i (Fig. 2C, blue curve), an effect that was visibly lowered upon mutation of the catalytic arginine finger (Fig. 2C, purple curve). However, a concentration-dependent increase in background P_i was also observed in the negative control containing heat-

denatured RAB-2 (Fig. 2C, orange curve). Because an isolated TBC domain cannot hydrolyze GTP autonomously, this baseline signal likely stems from either the partial, spontaneous refolding of a small RAB-2 subpopulation during the assay or the presence of trace, co-purified bacterial phosphatase contaminants in the TBC domain preparation. Due to this substantial background noise, it is inconclusive at this stage as to whether the observed differences between the wild-type and mutant enzymes are truly driven by a specific, TBC-mediated catalytic cycle.

Discussion

The spatial and temporal regulation of Rab GTPases is a fundamental mechanism driving vesicular transport and organelle identity. In the context of regulated secretion, the RAB-2 signaling serves as a critical checkpoint for the biogenesis and maturation of secretory granules (SGs), ensuring that specialized cargo is properly retained (Sumakovic et al., 2009; Edwards et al., 2009). While genetic evidence has implicated RUND-1 and TBC-8 acting alongside RAB-2 in this pathway, their precise biochemical mechanisms have remained elusive. In this study, we provide the first direct biochemical characterization of the RAB-2/RUND-1/TBC-8 machinery, establishing that TBC-8 acts as a bone fide GTPase-activating protein (GAP) for RAB-2 and demonstrating that RUND-1 functions as a negative regulator of this GAP activity.

Biochemical Confirmation of TBC-8 as a RAB-2 GAP

Although TBC-8 was previously identified as a putative GAP for RAB-2 (Hannemann et al., 2012), *in vitro* biochemical proof has been hindered by the difficulties of purifying full-length TBC-8. Despite experiencing low yields and significant degradation, our colorimetric malachite green assays successfully demonstrated that full-length MBP-TBC-8 accelerates the intrinsic GTP hydrolysis rate of RAB-2 in a dose-dependent manner (Fig. 1A).

RUND-1 as a Gatekeeper of RAB-2 Longevity

Adding purified RUND-1 to our reconstituted system suppressed TBC-8-mediated GTP hydrolysis in a robust, dose-dependent manner (Fig. 1B). This result suggests that RUND-1 behaves as a kinetic modulator that stabilizes the active state of RAB-2 by protecting it from GAP-mediated inactivation. Since RAB-2 cycling must be tightly restricted to a narrow spatiotemporal window at the trans-Golgi network (TGN) to successfully sort luminal and transmembrane cargo, any disruption to this clockwork will disrupt SG maturation. In *tbc-8* null mutants, hyper-activated or prolonged RAB-2-GTP signaling likely traps RAB-2 and its effectors on the membrane and prevents the efficient maturation and cargo retention of dense-core vesicles. Conversely, in *rund-1*

mutants, the lack of GAP inhibition would cause premature GTP hydrolysis, short-circuiting the active RAB-2 lifetime before cargo sorting is complete. Thus, RUND-1 acts as a molecular brake on TBC-8, ensuring that RAB-2 remains in its active, GTP-bound state long enough to orchestrate mature cargo packaging.

A Model for Spatiotemporal Coordination at the TGN

Based on our biochemical data and existing genetic studies, we propose a working model for RAB-2 regulation during secretory granule biogenesis. Upon recruitment and activation of RAB-2 at the TGN membrane, RUND-1 binds to the active GTPase, forming a stable heteromeric complex as supported by our mass distribution shifts (Fig. S1D). Simultaneously, RUND-1 acts as a regulatory scaffold, interacting with TBC-8 and sterically or conformationally shielding RAB-2 from TBC-8-mediated hydrolysis. This extended "on" state allows the recruitment of essential sorting machinery and the segregation of regulated secretory cargo. Once cargo packaging is secured, a trigger - potentially a conformational shift, post-translational modification, or the recruitment of an additional displacement factor - relieves RUND-1's inhibition, allowing TBC-8 to catalyze GTP hydrolysis and drive the pathway forward.

Future work will be essential to precisely map the binding interfaces within the RAB-2/RUND-1/TBC-8 complex and to examine RUND-1's inhibitory action. Additionally, optimization of the TBC domain purification to eliminate background phosphatase activity will be critical to fully confirm the kinetic parameters of the arginine finger mutant.

Materials and Methods

Protein Expression and Purification

The expression vector (pMA64) encoding intein-tagged RUND-1 was transformed into *E. coli* ER2566 cells for protein expression. Cells were grown in Terriffic Broth (TB) with ampicillin and chloramphenicol at 37°C until reaching an OD600 of 0.6–0.8, then shifted to 18°C, and induced with 0.5 mM IPTG for 18.5 hours. Harvested cells were resuspended in Buffer A (20 mM Tris-HCl (pH 7.6), 500 mM NaCl, 1 mM EDTA, 1 mM TCEP) containing 1 mM $MgCl_2$ and a protease inhibitor cocktail (Pierce), lysed via fluid homogenization (15,000 psi, 4 passes), treated with 1 mg/mL DNase I, and supplemented with 0.1% Triton X-100. The lysate was clarified at 30,000xg for 25 minutes and filtered (0.22 um). For affinity purification, the clarified lysate was batch-bound to chitin resin for 2 hours at 4°C. The resin was washed Buffer A. On column intein cleavage was initiated by washing with Buffer A supplemented with 50 mM DTT, followed by an overnight incubation at room temperature. The cleaved RUND-1 protein

was eluted with Buffer A, quantified via NanoDrop, and fractions were pooled and buffer-exchanged into storage buffer (20 mM HEPES, 160 mM KOAc, 1 mM MgOAc, 10% glycerol).

Recombinant GST-RAB-2, RAB-2-His8, and His6-SUMO-TBC domain were expressed in *E. coli* BL21(DE3) pLysS Rosetta cells (Invitrogen). Cultures were grown at 37°C in LB medium containing selection antibiotics (ampicillin/chloramphenicol) to an OD600 of 0.4–0.6. Expression was induced overnight at 18°C using 1 mM IPTG. Harvested cell pellets were resuspended in the respective ice-cold base lysis buffers outlined below:

- GST Lysis Buffer: 50 mM Tris (pH 7.6), 200 mM NaCl, 10% glycerol, 5 mM 2-mercaptoethanol, 2 mM $MgCl_2$.
- His Lysis Buffer: 50 mM Tris (pH 7.6), 200 mM NaCl, 10% glycerol, 5 mM 2-mercaptoethanol, 2 mM $MgCl_2$, supplemented with 10–25 mM imidazole to minimize non-specific background binding.

All base buffers were supplemented with 1uL Benzonase per 10 mL, 1 mM PMSF, and a protease inhibitor cocktail. Cells were mechanically lysed, and the crude lysates clarified similarly to RUND-1. For GST-RAB-2, the supernatant was batch-bound to GST-Sepharose resin (GE Healthcare) for 2 hours at 4°C. The glutathione column was washed with GST wash buffer (50 mM Tris (pH 7.6), 200 mM NaCl, 2 mM $MgCl_2$) followed by a high-salt wash (50 mM Tris (pH 7.6), 500 mM NaCl, 2 mM $MgCl_2$). Bound GST protein was eluted with elution buffer (50 mM Tris (pH 8.0), 200 mM NaCl, 2 mM $MgCl_2$, 10 mM reduced glutathione). For RAB-2-His8 and His6-SUMO-TBC domain, the supernatant was incubated with Ni-NTA Agarose resin. The Ni-column was washed with wash buffer (50 mM Tris (pH 7.6), 200 mM NaCl, 10% glycerol, 5 mM 2-mercaptoethanol) containing 25–35 mM imidazole. Target proteins were eluted using the same buffer supplemented with 250–400 mM imidazole. Finally, peak fractions for all constructs were pooled and buffer-exchanged into storage buffer (20 mM HEPES, 160 mM KOAc, 1 mM MgOAc, 10% glycerol).

GTP hydrolysis reaction

GTP hydrolysis reactions were assembled directly in the presence of free nucleotide. Standard reactions were prepared in triplicate on ice within a 96-well plate. Each well was set up in a final reaction buffer (20 mM HEPES (pH 7.5), 150 mM NaCl, 2 mM $MgCl_2$) supplemented with 1uM GTP.

The reaction mixtures contained 6uM purified GST-RAB-2 alone or in combination with varying concentration of the purified TBC domain (using either wild-type or the catalytic arginine finger mutant construct). Where indicated, purified RUND-1 was added to the mixture at concentrations 1uM to assess dose-dependent kinetic modulation.

Hydrolysis was initiated by shifting the assembled 96-well plate from ice to a 37°C incubator and incubating for 2 hours. Reactions were subsequently quenched to arrest further nucleotide cleavage by adding EDTA to a final concentration of 200 mM and immediately returning the plate to ice.

Malachite Green Assay

Frozen protein stocks were thawed on ice, and GTP hydrolysis reaction was assembled as described above. Reactions were prepared in triplicate on ice within a 96-well plate. Following a 2-hour incubation at 37°C, hydrolysis was quenched by adding 200 mM EDTA and shifting the plate back to ice.

Colorimetric detection of free P_i was performed by adding 200uL of a prepared malachite green reagent (0.034% (w/v) malachite green carbinol base, 1.0% (w/v) ammonium molybdate, and 1.0 N HCl) to each well. The mixtures were incubated at room temperature for 5 minutes, after which the optical density was recorded at 650 nm using a plate reader. Background phosphate levels from protein-free controls were subtracted from all samples. A potassium phosphate standard curve was used to calculate the P_i by GTP hydrolysis.

Mass Photometry

Mass photometry experiments were performed at room temperature using a TwoMP system (Refeyn Ltd) to evaluate the oligomeric states and binding interactions of RUND-1 and GST-RAB-2 or His_6SUMO-TBC domain and His_8-RAB-2. For single-protein analysis, freshly thawed protein stocks were diluted in cold assay buffer (20 mM HEPES (pH 7.5), 150 mM NaCl, 2 mM $MgCl_2$) to an intermediate concentration of 50 nM. This mixture was then diluted tenfold directly into a droplet of room-temperature assay buffer on the coverslip, yielding a final working concentration of 5nM for immediate measurement.

For protein-protein interaction assays involving GST-RAB-2 and RUND-1, GST-RAB-2 was nucleotide-loaded prior to complex assembly to stabilize its active conformation. GST-RAB-2 was pre-incubated with a 20-fold molar excess of GTP in loading buffer [20 mM HEPES (pH 7.5), 100 mM NaCl, 5 mM EDTA] for 30 minutes at 30°C to induce nucleotide exchange. The loading reaction was quenched by adding $MgCl_2$ to a final concentration of 10 mM to coordinate and lock the GTP molecule within the catalytic core. For protein-protein interaction assays (GST-RAB-2 with RUND-1, or RAB-2-His8 with His6-SUMO-TBC domain), the binding partners were pre-incubated on ice at an equimolar ratio to a concentration of 25nM each (50nM total protein concentration). This mixture was pre-incubated on ice for 10–15 minutes to allow complex formation,

followed by a final dilution into the room-temperature assay droplet to achieve a target complex concentration of 5nM.

Movies were recorded immediately following final sample dilution, capturing binding events at a rate of 600 frames/min for a duration of one minute. Molecular mass calibrations were established using a standard protein mixture (beta-amylase, apoferritin, and glutamate dehydrogenase) under identical buffer conditions. All data collection was executed using AcquireMP (v2.3) and subsequently analyzed with DiscoverMP (v2.3) software. To quantify and compare the relative populations of monomeric, oligomeric, and heterocomplex species, the absolute particle counts for each peak were determined by integrating the area under the curve of a Gaussian fit applied to the mass distribution histograms. Resulting counts were normalized to reflect the respective subunit stoichiometry of each species.

FIGURES

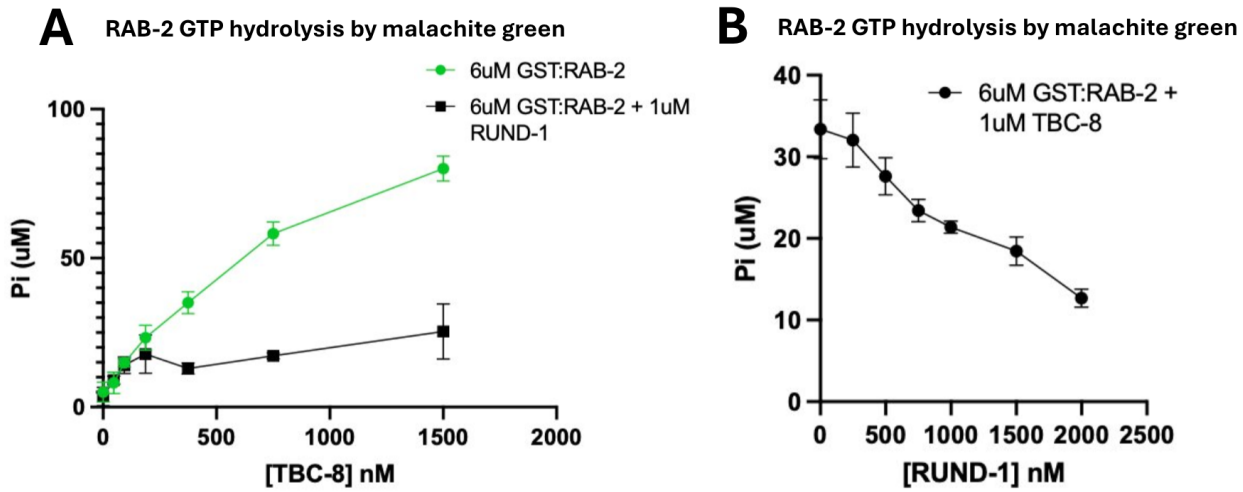

Figure 1. TBC-8 functions as a GAP for RAB-2 and is inhibited by RUND-1.

A. In vitro GTPase assay measuring the release of P_i from 6uM RAB-2. Addition of increasing concentrations of TBC-8 (blue line) significantly accelerates RAB-2 GTP hydrolysis, identifying TBC-8 as a RAB-2 GTPase-activating protein (GAP). The addition of 1uM RUND-1 (orange line) suppresses TBC-8-mediated hydrolysis, suggesting an inhibitory role for RUND-1, n = 3.

B. Dose-response curve of RUND-1 inhibition. Fixed concentrations of RAB-2 (6uM) and TBC-8 (1uM) were incubated with increasing concentrations of RUND-1. The linear decrease in P_i production confirms that RUND-1 inhibits the GAP activity of TBC-8 in a concentration-dependent manner, n = 3.

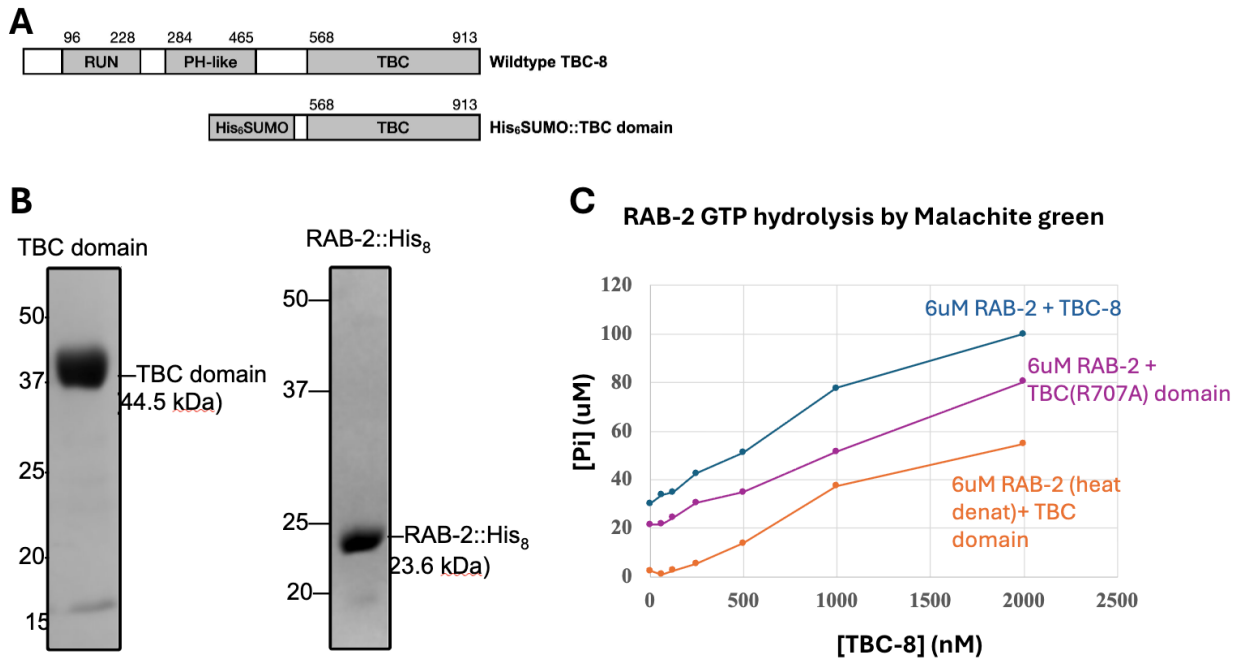

Figure 2. Characterization of TBC domain of TBC-8.

A. Schematic representation of full-length TBC-8 (top) and the truncated TBC domain construct (residues 568–913). The truncation was expressed as His_6-SUMO fusion protein and subsequently cleaved to yield the untagged TBC domain.

B. SDS-PAGE analysis of purified recombinant proteins. Left: Purified untagged TBC domain (44.5kDa). Right: Purified RAB-2-His_8 (23.6kDa)

C. *In vitro* GTPase assay of the TBC domain using the malachite green assay. 6uM RAB-2-His_8 was incubated with increasing concentrations of the TBC domain (blue line). The TBC(R707A) catalytic mutant was tested (purple line). Additionally, the TBC domain was incubated with heat-denatured RAB-2-His_8 (orange line) to assess background phosphate levels in the protein preparations.

SUPPLEMENTARY MATERIALS

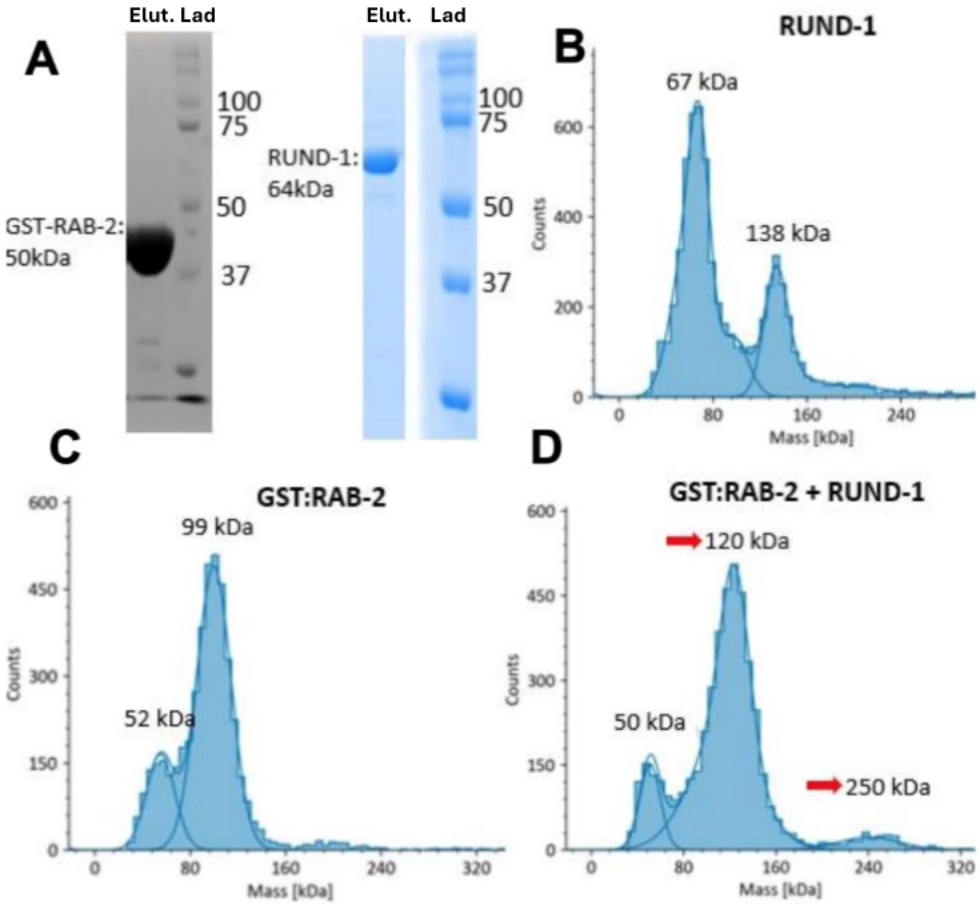

Figure S1. Interaction of purified RUND-1 and GST-RAB-2.

A. SDS-PAGE analysis of purified recombinant GST-RAB-2 (50kDa) and RUND-1 (64kDa). Eluates (Elut.) were resolved alongside molecular weight markers (Lad).

B. Mass Photometry (MP) histogram of RUND-1. The primary peak at 67kDa corresponds to a RUND-1 monomer, while the secondary peak at 138kDa indicates the presence of a homodimer, n = 3.

C. MP histogram of GST-RAB-2. The observed peak at 99kDa suggests that GST-RAB-2 predominantly exists as a homodimer in solution, consistent with the known dimeric nature of the GST tag, n = 3.

D. MP histogram of a stoichiometric mixture of GST-RAB-2 and RUND-1. The shift in mass distribution and the appearance of peaks at approximately 120kDa and 250kDa (red arrows) suggest the formation of higher-order complexes between RAB-2 and RUND-1, supporting a direct physical interaction, n = 3.

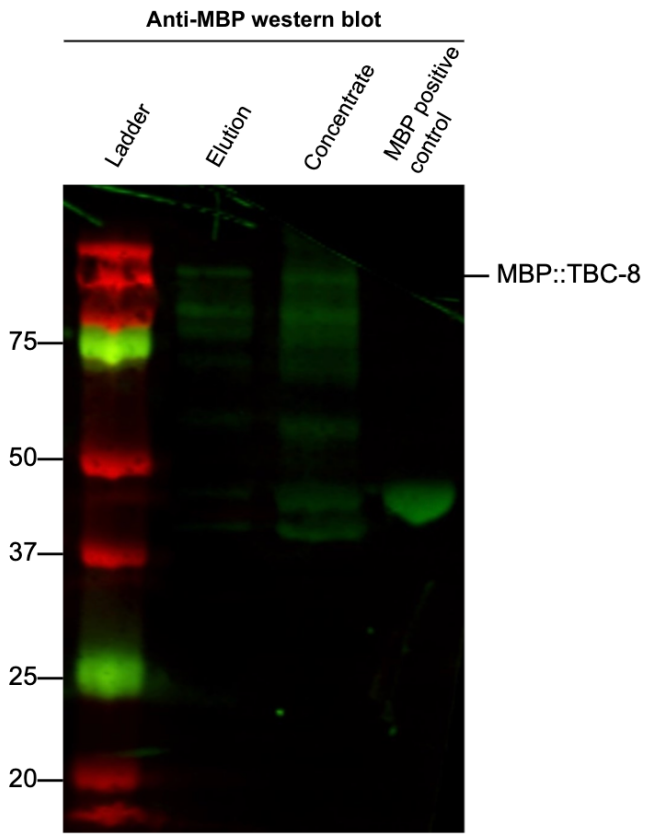

Figure S2. Expression and purification analysis of MBP::TBC-8. Immunoblot analysis using an anti-MBP antibody confirms the presence of the fusion protein. The molecular weight ladder (left lane) indicates protein sizes in kilodaltons (kDa). The "Elution" and "Concentrate" lanes exhibit a band corresponding to the expected molecular weight of full-length MBP::TBC-8 (145kDa), alongside lower molecular weight degradation products. An MBP-only positive control (right lane) is resolved at approximately 42 kDa to validate antibody specificity and blotting efficiency.

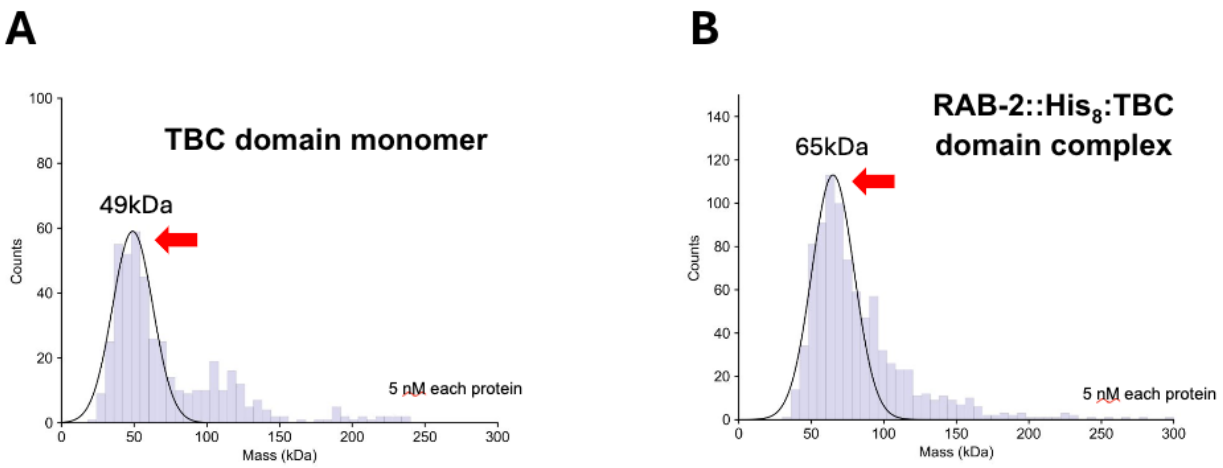

Figure S3. Biophysical validation of the TBC domain and RAB-2 complex formation.

A. MP histogram of the purified TBC-8 TBC domain. The primary peak observed at 49kDa (red arrow) is consistent with the predicted molecular weight of the TBC domain monomer (44.5kDa), confirming it is primarily monomeric in solution, n = 3.

B. MP histogram of a stoichiometric mixture of the TBC domain and RAB-2-His_8. The shift of the main population to a peak at 65kDa (red arrow) corresponds to the combined molecular weight of the TBC domain (44.5kDa) and RAB-2-His_8 (23.6kDa), indicating the formation of a 1:1 heterodimeric complex. Data were collected at room temperature in a physiological buffer, n = 3.

REFERENCES

Caro, Lucien G., and George E. Palade. "Protein Synthesis, Storage, and Discharge in the Pancreatic Exocrine Cell: An Autoradiographic Study." *Journal of Cell Biology*, vol. 20, no. 3, Mar. 1964, pp. 473–95. *SAGE Journals*, https://doi.org/10.1083/jcb.20.3.473.

Cazares, VA, et al. "Distinct Actions of Rab3 and Rab27 GTPases on Late Stages of Exocytosis of Insulin." *Traffic*, vol. 15, no. 9, Sept. 2014, pp. 997–1015. *Wiley Online Library*, https://doi.org/10.1111/tra.12182.

Edwards, S. L., et al. "Impaired Dense Core Vesille Maturation in *Caenorhabditis elegans* Mutants Lacking Rab2." *Journal of Cell Biology*, vol. 186, no. 6, 21 Sept. 2009, pp. 881–95. *Rockefeller University Press*, https://doi.org/10.1083/jcb.200902095.

Hannemann, M., et al. "TBC-8, a Putative RAB-2 GAP, Regulates Dense Core Vesicle Maturation in *Caenorhabditis elegans*." *PLoS Genetics*, vol. 8, no. 5, May 2012, p. e1002722. *Public Library of Science*, https://doi.org/10.1371/journal.pgen.1002722.

Jamieson, James D., and George E. Palade. "Intracellular Transport of Secretory Proteins in the Pancreatic Exocrine Cell: I. Role of the Peripheral Elements of the Golgi Complex." *Journal of Cell Biology*, vol. 34, no. 2, 1 Aug. 1967, pp. 577–96. *SAGE Journals*, https://doi.org/10.1083/jcb.34.2.577.

Matsunaga, K., et al. "Rab2a and Rab27a Cooperatively Regulate the Transition from Granule Maturation to Exocytosis Through the Dual Effector Noc2." *Journal of Cell Science*, vol. 130, no. 3, 1 Feb. 2017, pp. 541–50. *The Company of Biologists*, https://doi.org/10.1242/jcs.195479.

Neuman, S. D., et al. "A Novel Function for Rab1 and Rab11 During Secretory Granule Maturation." *Journal of Cell Science*, vol. 134, no. 15, 1 Aug. 2021, p. jcs259037. *The Company of Biologists*, https://doi.org/10.1242/jcs.259037.

Nickerson, D. P., et al. "Termination of Isoform-Selective Vps21/Rab5 Signaling at Endolysosomal Organelles by Msb3/Gyp3." *Traffic*, vol. 13, no. 10, Oct. 2012, pp. 1411–28. *Wiley Online Library*, https://doi.org/10.1111/j.1600-0854.2012.01390.x.

Pan, X., et al. "TBC-Domain GAPs for Rab GTPases Accelerate GTP Hydrolysis by a Dual-Finger Mechanism." *Nature*, vol. 442, no. 7100, 20 July 2006, pp. 303–06. *Nature Publishing Group*, https://doi.org/10.1038/nature04847.

Pfeffer, Suzanne R. "Rab GTPases: Master Regulators That Establish the Secretory and Endocytic Pathways." *Molecular Biology of the Cell*, vol. 28, no. 6, 15 Mar. 2017,

pp. 712–15. *American Society for Cell Biology*, https://doi.org/10.1091/mbc.E16-10-0737.

Sumakovic, M., et al. "UNC-108/RAB-2 and Its Effector RIC-19 Are Involved in Dense Core Vesicle Maturation in *Caenorhabditis elegans*." *Journal of Cell Biology*, vol. 186, no. 6, 21 Sept. 2009, pp. 897–914. *Rockefeller University Press*, https://doi.org/10.1083/jcb.200902096.

CHAPTER 4

FUTURE DIRECTIONS

1. Generation of RUNDC1KD cells using CRISPR Cas9

While our lab has successfully utilized CRISPR-Cas9 to knockout other components of SG biogenesis pathway - including *Ccdc186* and *Eipr1* - generating a complete *Rundc1* knockout (KO) in INS-1-derived 832/13 cells has been exceptionally challenging. We employed two distinct genome-editing strategies: a plasmid-based expression system and a delivered ribonucleoprotein (RNP) complex approach.

Initially, we utilized a plasmid-based approach delivering the pSpCas9(BB)-2A-GFP vector targeting either the first or fourth exon of rat *Rundc1* (Figure 1A), co-transfecting a puromycin resistance plasmid (pPUR) for antibiotics selection. Screening of 16 individual RNP clones revealed that while 4 colonies were successfully edited, all 4 demonstrated a persistent heterozygous pattern, retaining the wild-type allele alongside the deletion band. This strongly suggested that editing occurred at only a single copy of the *Rundc1* locus.

To bypass potential limitations of plasmid-based expression - such as prolonged Cas9 expression leading to toxicity or off-target effects, or low transfection efficiency - we switched to a direct ribonucleoprotein (RNP) delivery method. We dual-targeted distinct exons simultaneously using Cas9 protein complexed with two sgRNAs, aiming to induce a frame-shift mutation. Initial screening of 28 RNP clones recapitulated our plasmid-based results: 4 clones successfully demonstrated the targeted deletion, but only on a single allele (Figure 1B). To achieve a complete knockout, we subjected one of these confirmed heterozygous clones to a second round of RNP-CRISPR targeting. However, PCR analysis of 55 subsequent colonies failed to yield a homozygous mutant, again yielding only heterozygous profiles. Characterization of these clones was further complicated by limitations in our immunodetection reagents. Western blot analysis using the available RUNDC1 antibody consistently yielded a non-specific, multi-band pattern preventing reliable phenotypic verification at the protein level (Figure 2).

While gene essentiality is a common driver of persistent heterozygosity, several lines of evidence suggest that a complete loss of RUNDC1 may not be lethal in INS-1 832/13 cell line. First, our laboratory has successfully generated viable knockout lines for *Ccdc186* and *Eipr1*, which operate in the same parallel genetic pathway. Second, *rund-1* null mutant lines in *C. elegans* are viable and fully capable of propagation, indicating that the core functional pathway is not strictly required for organismal or cellular survival. Our guide RNA designs also demonstrated high targeting efficiency - as

evidenced by the successful cleavage and deletion events observed in the isolated heterozygous clones.

Hence, the aneuploid or polyploid nature of the 832/13 cell line represents the most plausible obstacle. Future work should pair the RNP delivery approach with Fluorescence In Situ Hybridization (FISH). By utilizing locus-specific fluorescent probes alongside genomic sequencing, we can definitively determine the baseline copy number of the *Rundc1* gene in our specific cell line, quantify the exact multi-allelic editing efficiency, and estimate number of colonies required to screen to isolate a null mutant.

2. Does RUNDC1 directly control proinsulin trafficking or operate through an intermediate cargo?

While the (pro)CpepSNAP assay reveals a striking cargo export defect in RUNDC1-knockdown cells, it remains unclear whether RUNDC1 is directly involved in the physical mechanics of vesicle trafficking, or if the budding granules simply lack an essential sorting factor required to trigger efficient TGN detachment. To distinguish these models, I propose an acute protein relocation strategy such as knock-sideways, which uses a chemical trigger to mechanically sequester RUNDC1 away from its native TGN post to a different organelle such as mitochondria. If acute depletion of RUNDC1 at the Golgi face causes an immediate freeze of the pre-loaded (pro)CpepSNAP wave, the results will demonstrate that RUNDC1 functions as a direct, active structural component of the vesicle budding or transport machinery. Conversely, if the (pro)CpepSNAP granules exit the TGN normally despite the sudden absence of RUNDC1, t will support that RUNDC1 affects trafficking by dictating nascent granule composition, wherein the granules simply fail to accumulate a necessary factor to exit the TGN.

3. Optimization of Full-Length TBC-8 Purification

Our biochemical analysis shows that RUND-1 slows down TBC-8-mediated GTP hydrolysis on RAB2. However, a persistent technical limitation was the low yield and structural instability of full-length bacterial recombinant TBC-8, preventing further analysis of protein-protein interactions. I propose using the mammalian expression systems, specifically HEK293T cells, to purify full-length TBC-8. Mammalian hosts provide essential post-translational modifications and chaperone environments that may significantly improve the stability, solubility, and yield of the full-length protein.

4. Structure-Guided Mutagenesis of the RUND-1 RUN Domain

While our mass photometry (MP) data confirms that RUND-1 forms a stable physical assembly with active RAB-2, the precise molecular interface remains to be discovered. RUND-1 interacts with RAB-2 via its conserved, N-terminal RUN domain. To identify the exact residues governing this interaction, I propose a strategy utilizing sequence/homology alignments based on recently characterized mammalian RUN-domain/GTPase structures, such as the RUSC2:RAB35 complex (Lin et al, 2019). By mapping the conserved electrostatic and hydrophobic contact surfaces of the RUSC2:RAB35 structural interface onto the RUND-1 sequence, targeted point mutations can be designed within the RUND-1 RUN domain. Future investigations can validate these candidates *in vitro* using MP to determine if the engineered point mutations successfully abolish the physical interaction with RAB2. Expressing these binding-deficient constructs in *C. elegans rund-1* mutants will reveal their ability to rescue characteristic locomotion and secretory granule biogenesis defects, thereby determining whether this physical interaction is strictly required for RAB-2 pathway function *in vivo*.

FIGURES

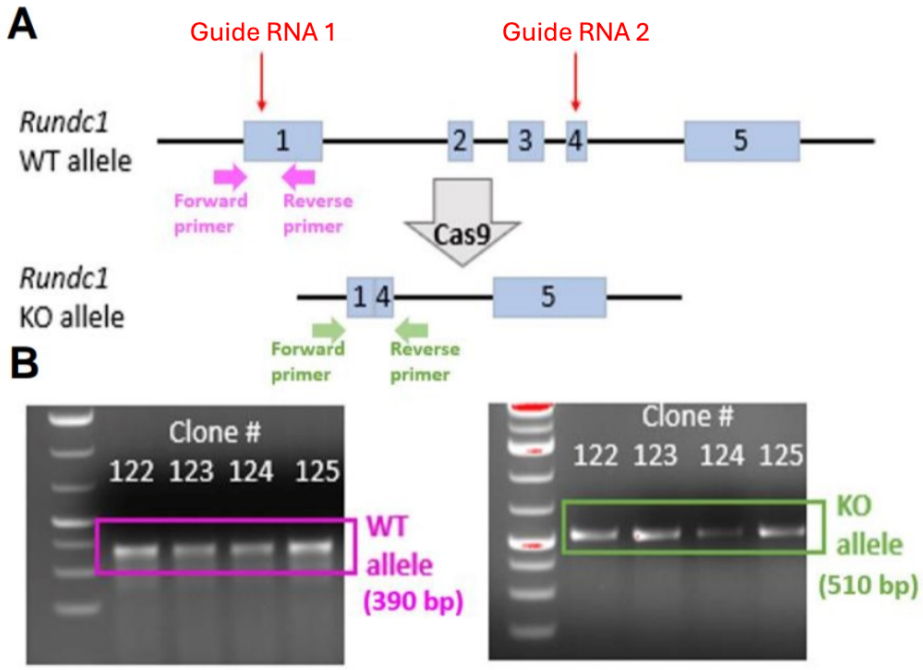

Figure 1. **CRISPR-Cas9 Strategy and Genotypic Analysis of *Rundc1* Targeting in 832/13 Cells.**

A. Schematic representation of the dual-guide RNA targeting strategy. The wild-type (WT) rat *Rundc1* genomic locus consists of 5 exons (blue boxes). Red arrows indicate the cleavage sites targeted by Guide RNA 1 (exon 1) and Guide RNA 2 (exon 4) using delivered CRISPR-Cas9 ribonucleoprotein (RNP) complexes. Successful dual-site cutting and structural repair result in a large genomic deletion encompassing exons 1 through 4, generating a truncated *Rundc1* knockout (KO) allele. Magenta arrows indicate the binding locations of the WT-specific primer set (flanking the exon 1 target site); green arrows indicate the binding locations of the KO-specific primer set designed to span the newly formed junction following excision.

B. PCR screening of isolated single-cell clones. Genomic DNA extracted from four representative clones (#122, 123, 124, and 125) was evaluated using the distinct primer sets detailed in (A). *Left panel:* Amplification with WT-specific primers yields a persistent 390 bp band across all samples, demonstrating that a wild-type copy of the *Rundc1* gene remains intact. *Right panel:* Amplification with KO-specific primers yields a 510 bp fragment across the same clones, confirming successful Cas9-mediated fragment deletion on at least one allele. The concurrent presence of both distinct bands indicates a stable, heterozygous editing profile across all isolated colonies.

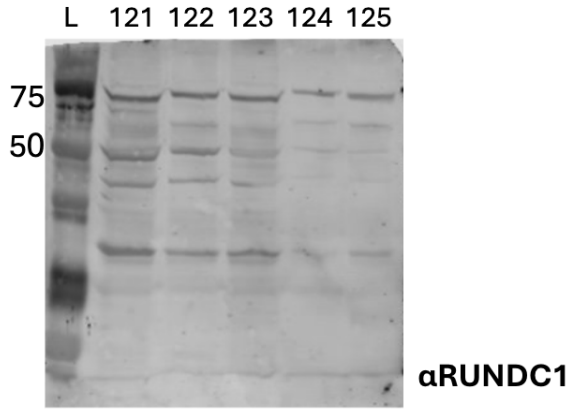

Figure 2. Western blot of whole-cell lysates harvested from representative single-cell 832/13 clones (#121–125) following RNP-mediated CRISPR-Cas9 genome editing. Immunoblot probed with an anti-RUNDC1 antibody reveals a non-specific multi-band profile across all analyzed samples, preventing definitive phenotypic identification or quantification of protein knockdown.

REFERENCES

1. Cattin-Ortolá, Jérôme, et al. "CCDC186 Controls Dense-Core Vesicle Cargo Sorting by Exit." *bioRxiv*, 2019, https://doi.org/10.1101/616458.

2. Lin, Lin et al. “Rab35/ACAP2 and Rab35/RUSC2 Complex Structures Reveal Molecular Basis for Effector Recognition by Rab35 GTPase.” *Structure (London, England : 1993)* vol. 27,5 (2019): 729-740.e3. doi:10.1016/j.str.2019.02.008.